PUBLICATIONS OF THE ASTRONOMICAL SOCIETY OF THE PACIFIC, **123**:1188–1209, 2011 October

Hectochelle: A Multiobject Optical Echelle Spectrograph for the MMT

ANDREW SZENTGYORGYI, GABOR FURESZ, PETER CHEIMETS, MAUREEN CONROY, ROGER ENG, DANIEL FABRICANT, ROBERT FATA, THOMAS GAURON, JOHN GEARY, BRIAN MCLEOD, JOSEPH ZAJAC, STEPHEN AMATO, HENRY BERGNER, NELSON CALDWELL, ANDREA DUPREE, RICHARD GODDARD, EVERETT JOHNSTON, SOEREN MEIBOM, DOUGLAS MINK, MARIO PIERI, JOHN ROLL, SUSAN TOKARZ, AND WILLIAM WYATT

Optical and Infrared Division, Harvard-Smithsonian Center for Astrophysics, 60 Garden St., Cambridge, MA 02138,

HARLAND EPPS

Lick Observatory, University of California, Santa Cruz, Santa Cruz, CA 95064,

LEE HARTMANN

Department of Astronomy, University of Michigan, Ann Arbor, MI 48109

AND

SZABOLCZ MESZAROS

Department of Optics and Quantum Electronics, University of Szeged, Szeged, Hungary

Received 2010 December 13; accepted 2011 August 9; published 2011 September 20

ABSTRACT. The Hectochelle is an optical band, fiber-fed, multiobject echelle spectrograph deployed at the MMT Observatory on Mount Hopkins, Arizona. The optical fibers that feed the Hectochelle are positioned by the Hectospec robot positioner on the MMT f/5 focal surface, and the Hectochelle shares an optical fiber feed system with the Hectospec, a moderate-dispersion spectrograph that is collocated with the Hectochelle. Hectochelle can record up to 240 spectra simultaneously at a resolution of 38,000. Spectra cover a single diffractive order that is approximately 150 Å wide. The total potential operating passband of the Hectochelle extends from 3800 Å to 9000 Å. Operated in conjunction with the MMT f/5 secondary, the MMT wide-field corrector, and the atmospheric dispersion compensator, the patrol field is 1° in diameter and the individual fiber slits are 1.5″ in diameter. The throughput of the combined telescope, fiber feed, and spectrograph is measured to be 6.1% at 5275 Å, exclusive of atmospheric extinction. A 20 minute observation of a $V = 15$ F-type star yields a signal-to-noise ratio of 35 per resolution element. Hectochelle had first light 2003 December 4 and continues to be operated at the MMT today.

Online material: color figures

1. INTRODUCTION

Many of the frontier problems in stellar astrophysics, especially studies of star formation and young stellar associations, involve observations of dense, clustered aggregations of similar objects with angular scales of a few degrees in extent. These observations are particularly amenable to multiobject techniques, where a high multiplex advantage leverages the investment in and the capabilities of large-aperture ground-based telescopes that have seen first light in the last 20 years. This multiplier can boost productivity of these precious observational assets by factors of 100 or more. Despite these ripe science opportunities, high-dispersion multiobject spectrographs suitable for these investigations are relatively rare. The commissioning of Hectochelle in 2003 added to the small census of high-dispersion, optical multiobject spectrographs, now consisting of Hydra (Bershady et al. 2008), Michigan/MIKE Fiber System (Walker et al. 2007), Giraffe (Avila et al. 2003), and Hectochelle (this article).

Hectochelle is an optical band, fiber-fed, multiobject echelle spectrograph deployed at the 6.5 m MMT Observatory on Mount Hopkins, Arizona. The Hectochelle is fed with 240 fibers from the Hectospec robot positioner. While the aperture of the MMT is somewhat smaller than some other modern large-aperture facilities, the efficiency of the Cassegrain focus, with no tertiary mirror, and an overall system design that was purposed to multiobject spectroscopy from its inception means that the moderate aperture size is compensated by other factors.

The design and implementation of Hectochelle was driven by requirements to the efficiency of the MMT and maximize wavelength stability. A choice was made to optimize performance in a wavelength band that includes the Ca H and K lines (3969 and

3933 Å), as well as the Hα (6563 Å), which embraces the Mg triplet (5167–5184 Å). Performance is preserved at the red end to 9000 Å, where strong telluric absorption features reduce atmospheric transmission significantly. By minimizing the number of optical surfaces in the telescope-spectrograph optical train, Hectochelle has very high throughput and thus is capable of a broad range of observational programs investigating objects throughout the Local Group and beyond. Special attention has been paid to the design and implementation of all optical coatings to further maximize efficiency. The relatively high resolution of Hectochelle ($R \sim 38,000$) was chosen to permit detailed abundance studies and, coupled with wavelength-scale stability, to enable good radial velocity precision (~100 m s^{-1}). While the Hectochelle user community has focused on stellar astrophysics, Hectochelle has also been used as a wide-field IFU for the study of extended objects—for example, the Mira H I trail and the cloud structure toward M15 in Na D.

As the cost and complexity of ground-based astronomical instrumentation has grown in recent years, the design process is often preceded by a flowdown from prime science drivers to physical parameters and thence to tolerances and error budgets. However, Hectochelle was conceived as a general-purpose instrument for which the design resolution was adopted a priori. Throughout the subsequent design process, the instrument team sought to maximize system throughput and wavelength-scale stability within the framework of budget constraints.

The Hectochelle records a single diffractive order at a time, since the second dimension of the CCDs that constitute the focal plane is used to spatially separate the individual fiber slits. The wavelength coverage of each order is approximately 150 Å. A resolution element is sampled in 5 pixels along dispersion; however, the density of this sampling may be reduced by on-chip binning during readout to increase the signal-to-noise ratio (S/N).

The overlapping diffractive orders are selected with order-sorting interference filters. The passbands of these filters are approximately one free spectral range wide and generally centered on the individual-order free spectral ranges. The total potential operating passband of Hectochelle is 3800 Å to 9000 Å, limited in the blue by the transmission of the optical fibers that feed the Hectochelle and in the red by the quantum efficiency of the focal-plane CCDs.

In a 20 minute observation of 15th magnitude F-type star, a S/N of 35 per resolution element is obtained. Radial velocity measurement repeatability of 100 m s^{-1} has been demonstrated on high-S/N solar spectra for long time baselines (e.g., 7 months). Day-to-day repeatability of 40 m s^{-1} was achieved. At the faint limit, velocity precision of ~2 km s^{-1} has been achieved on 21st magnitude red giant branch (RGB) stars in Local Group dwarf spheroidal galaxies in 3 hr. A computer-aided-design rendering of Hectochelle is shown in Figure 1. The gross parameters of Hectochelle are listed in Table 1.

A preconstruction review of Hectochelle's properties can be found in Szentgyorgyi et al. 1998; this article describes its post-construction properties and performance. In § 2, we describe the interface to the MMT telescope and the Hectospec robot positioner. Section 3 is a description of the optical design. The mechanical design aspects of Hectochelle are discussed in § 4. The instrument electronics are covered in § 5. Thermal control of the Hectochelle environment is discussed in § 6. The control software for Hectochelle is described in § 7. The calibration system is discussed in § 8. Operational aspects of using Hectochelle are covered in § 9. In § 10, we describe the instrument performance. Section 11 contains a description of several illustrative observational programs undertaken using Hectochelle. Section 12 contains a short discussion, some conclusions, and future plans for Hectochelle.

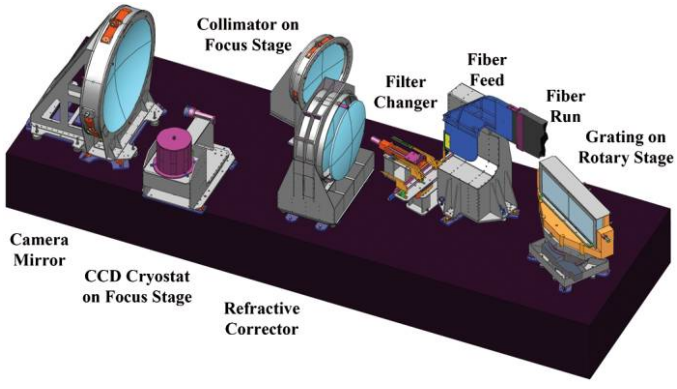

FIG. 1.—Mechanical layout of Hectochelle spectrograph. See the electronic edition of the *PASP* for a color version of this figure.

2. INTERFACES TO THE MMT AND THE HECTOSPEC ROBOT POSITIONER

Hectochelle is operated at the f/5 focus of the MMT that is corrected to a 1° diameter, curved field of view with a refractive, wide-field corrector that consists of a triplet of all-spherical,

TABLE 1
PARAMETERS OF HECTOCHELLE SPECTROGRAPH

Parameter	Value
Resolution	38,000
Efficiency	6%
Multiplex	240 fibers
Camera design	Catadioptric
Passband	3800–9000 Å
Single-order passband	~150 Å
Resolution element	6 (disp.) × 10 (spat.) pixels
Input focal ratio	5.4
Grating pitch	110 lpm
Blaze angle	64.5° (R2)
Opening angle α-β	15°
Anamorphic factor	0.56
Demagnification	0.49
Input fiber spacing	480 μm

fused-silica lenses (Fata et al. 2004; Fabricant et al. 2004). Atmospheric dispersion is also corrected with an atmospheric dispersion compensator consisting of a pair of counter-rotating, zero-deviation prisms. These optical elements are all coated with SolGel (Bohn & Leist 1998), so the peak transmission of the entire optical train at 5100 Å is essentially 100% when freshly coated, falling to 89% at the ends of the operating passband at 3600 Å and 9000 Å. The f/5 focus has a dedicated, deployable Shack-Hartmann wavefront sensor (Pickering et al. 2004), which patrols the full field of view of the wide-field corrector. The plate scale at f/5 is 170 μm arcsec^{-1} averaged over the entire field, so the 250 μm diameter core optical fibers that feed Hectochelle subtend 1.5″ on the sky. The total slit length is 6′ on the sky.

The Hectospec robot positioner arranges optical fibers on the curved f/5 focal surface and can position all 300 optical fibers in 5 minutes with 25 μm (0.14″) accuracy. Adjacent fibers can be spaced as closely as 20″; however, positioning constraints are complicated due to the tube connecting each fiber button to the edge of the focal surface positioner. The optical fiber run between the robot and Hectochelle is 26 m long. The Hectochelle shares the robot positioner and fiber feed system with the Hectospec, a moderate-dispersion spectrograph that is deployed in the same instrument room as Hectochelle at the MMT. Since Hectospec has greater reduction than Hectochelle, Hectochelle only accesses 240 of the 300 Hectospec optical fibers. The Hectospec spectrograph and robot positioner are discussed fully in Fabricant et al. (1994, 2005).

3. THE HECTOCHELLE OPTICAL DESIGN

3.1. Optical Design Overview

Hectochelle is a Schmidt-geometry spectrograph. In a Schmidt design, the slit is curved and lies on a circle that is concentric with the radius of curvature of the spherical collimator and has exactly $\frac{1}{2}$ the radius of curvature of the collimator. In Hectochelle, the slit is a linear array of optical fibers, i.e., a fiber slit. The echelle grating is centered on common center of curvature of the Schmidt system; hence, the collimator forms a pupil on the grating. The camera design is catadioptric with an internal focus that is a variant of the HIRES camera design (Epps & Vogt 1993). The optical layout of the Hectochelle appears in Figure 2.

The spectrograph beam size is 254 mm and the spectrograph input focal ratio is f/5.4. A doublet refractive corrector provides aberration compensation. The reduction of the spectrograph is 0.49. The optical surfaces are all-spherical. The prescription for the Hectochelle appears in Table 2.

The curved Schmidt-geometry slit is formed by fanning out the fibers in the fiber "shoe"—the mechanical interface between the fiber run and the spectrograph—so that the radius of curvature of the slit conforms to the Schmidt symmetry condition and the output beam of the fibers is normal to the local radius of curvature of the Schmidt geometry. The center-to-center distance between the fibers in perpendicular to the dispersion direction is 0.480 mm and the fiber-to-fiber angular divergence is 0.04°. The input to the fibers at the telescope focal plane is f/5.4, but focal-ratio degradation will tend to reduce the output focal ratio somewhat. For this reason, the fiber output is masked to f/5.4 with an aperture at the pupil formed on the echelle grating. The exact amount of light that is masked out depends slightly on the focal-ratio degradation, which varies from fiber to fiber and the orientation of the telescope, but a typical loss of 8% is to be expected.

The camera is catadioptric with a doublet refractive corrector and a spherical mirror. The corrector lens elements are also all spherical. The vacuum window of the cryostat has power and also functions as a field flattener. The fused-silica corrector lenses are quite large (716.3 mm and 688.34 mm in diameter) and were fabricated by Goodrich Danbury Optical Systems, Inc.

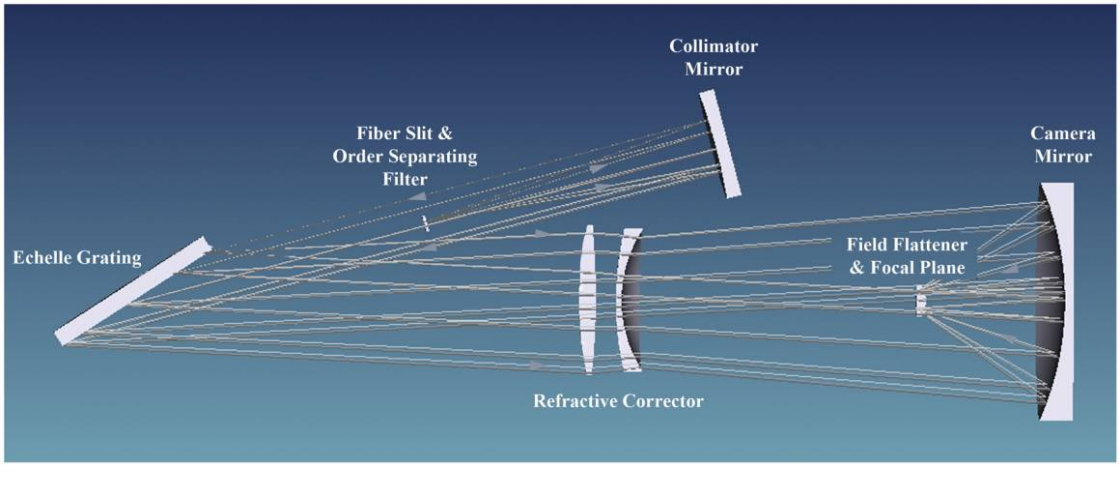

FIG. 2.—Optical layout of Hectochelle. See the electronic edition of the *PASP* for a color version of this figure.

TABLE 2
PRESCRIPTION OF HECTOCHELLE SPECTROGRAPH

Optic	Radius of curvature[a] (mm)	Diametral clear aperture (mm)	Material	Thickness (mm)
Slit	1375.11CX	…	…	1367.45
Collimator	2737.10 CC	591.82	Mirror	−2736.85
Grating	Infinity	…	Ruling-110 lpm	2032.00
Corr. lens 1	1670.34 CX	703.58	Fused silica	76.26
Corr. lens 1	3267.71 CX	…	…	92.53
Corr. lens 2	1458.06 CX	675.39	Fused silica	25.34
Corr. lens 2	590.83 CC	…	…	2038.27
Camera mirror	1350.99 CC	1060.45	Mirror	−638.88
Field flattener	131.45 CX	144.92	Fused silica	−40.64
Field flattener	494.26 CC	…	…	−9.92
Focal plane	Infinity	…	CCD	…

[a] CX indicates a convex surface and CC indicates a concave surface.

The substrates were Corning 7940, grade 5 F, procured directly from Corning Inc., Fused Silica Sales.

The focal ratio of the 1060 mm diameter camera mirror and 1351 mm radius of curvature result in an extremely deep concave figure. The monochromatic subapertures of individual monochromatic beams are elliptical (-436.9×243.8 mm)—so the effective focal ratio is approximately f/2.0. The camera has an internal focus.

The vignetting function is complicated, depending on the location within a given order, how high the beam is above or below the optical axis of the spectrograph, and weakly on the operating angle of the grating. The elements that contribute to vignetting are the fiber slit, a 15 mm gap between the grating facets, and the obscuration of the internal dewar. The internal dewar is by far the leading contributor to vignetting. On axis this vignetting is 22%. At half the maximum field angle it is 18%, and for beams near the edge of the CCD format, vignetting drops to 10%.

3.2. Order-Sorting Filters

Since Hectochelle is not cross-dispersed, the degeneracy of overlapping diffractive orders is lifted with the order-sorting filters. The passband of these filters is typically one free spectral range wide for a given order. These filters are realized with a combination of colored glass and interference layers. We required the filters to have high in-band transmission and to meet tight specifications. Furthermore, the size and aspect ratio of the filters—their clear aperture is a 7.5×82 mm rectangle—proved challenging to potential fabricators. For these reasons, the order-sorting filters were relatively expensive. Twenty-five filters would be required to span the prime Hectochelle orders (orders 18 to 42, or ~3800Å–9300Å); however, only a subset of these filters was actually purchased. The properties of these filters are tabulated in the Appendix.

Ideally, the order-sorting filters would have been curved to match the curvature of the fiber slit. This would have guaranteed normal incidence of all fiber output beam on the filter, so angle-dependent shifts of the passband center wavelength and transmission would be reduced to effects due to the divergence of the beam output from the fibers. Since curved substrates were clearly too expensive, we explored the effect of flat filters. While a single filter was found to produce an unacceptable wavelength shift at its extremities where the angle of incidence deviated significantly from the surface normal, approximating the ideal curved surface with two flat, tangent filters met our requirements, so each order is sorted with a pair of filters. The maximum angle between the optical beam and the filter surface normal is approximately 30 μrad.

3.3. Echelle Grating Optical Properties

The grating is a mechanically fixtured mosaic of two Richardson Grating Laboratory gratings with 302×410 mm clear apertures. Each grating has a 5 mm thick null border and there is a 5 mm mechanical gap between the two grating tiles. The ruling density is 110 lines per millimeter and the rulings are blazed at 64.5°. The incident and central diffracted beams that intersect the grating face have an opening angle of 15°. The angle of incidence (α) is 72° and the center-wavelength diffraction angle (β) is 57°. The anamorphic factor ($\cos(\alpha)/\cos(\beta)$) is 0.56, so the slit image of the 250 μm circular fiber ends are imaged as ellipses with 124 μm × 69 μm major and minor axes at the focal plane. The minor axis is approximately aligned with the dispersion direction, thus boosting resolution by an amount equal to the anamorphic factor. At the CCD pixel pitch of 13.5 μm, the sampling is 9.1×5.1 pixels. The opening angle of the beams incident on the grating in the spatial direction is $\pm 2.58°$ with respect to the optical axis of the spectrograph.

3.4. Imaging Performance and Format

The geometry of the focal plane is illustrated in Figure 3. While we have butted the CCDs that constitute the focal plane

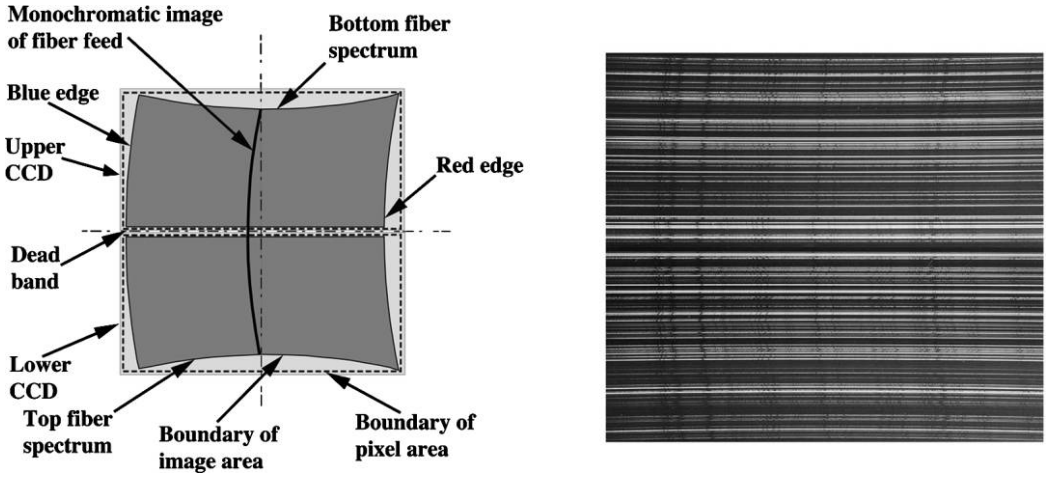

FIG. 3.—Focal-plane layout showing sense of pincushion and out-of-plane order distortions. A schematic of a how the spectra fall on the focal CCD focal plane when various distortions are taken into account appears in the left panel. An actual Hectochelle CCD image appears on the right. The dispersion direction is right–left in both cases.

as closely as possible, there is a residual 1.27 mm gap or "dead band" between the two mosaicked CCDs (see Fig. 3). The columns (i.e., the long dimension of the CCD) are aligned with the dispersion direction so there is no gap in the wavelength coverage. This gap is mirrored onto the spacing of the fibers on the fiber slit, so no fiber images "fall into the crack." The center-to-center spacing of the fibers in the fiber shoe is 480 μm, which corresponds to 235 μm on the focal plane. This spacing provides a 7 pixel null between the individual fiber spectra.

The spacing of the 240 spectra provides a very deep null between individual spectra at the full-resolution (unbinned) mode, although distance between neighboring orders varies slightly between values of 16–18 pixels. This is due to small irregularities of fiber placement within the fiber shoe. Since the FWHM of a spectrum perpendicular to dispersion is 10 pixels, the interorder separation is therefore 6 to 8 pixels. Good background sampling between orders is achievable, and there is no cross-talk between the spectra. In fact, this interorder area is used for measuring the background and scattered light: when a given order is traced during extraction, the background levels are measured in a narrow stripe at a given distance from the central trace of the order at either side. The level of scattered light varies across the focal plane between 0.1 and 0.2%.

When binned by 2×2 pixels, slight cross-talk between the closest apertures can occur. However, this is usually not an issue, since such binning mode is mostly used for fields with fainter objects, for which the S/N is very low in the wings of the spectra.

The fiber slit images on the focal plane exhibits mild pincushion and inevitable aberrations arising from the fact that the grating is operated in an out-of-plane configuration for all orders other than those on-axis (Fig. 3). These aberrations have been exaggerated in the drawing on the left of Figure 3. The actual amplitude of pincushion and color can be seen the real data in the right panel of Figure 3. Pure pincushion is seen as bowing of the spectra in the up-down direction. The out-of-plane effect is seen as bowing of absorption features in the right-left direction. Out-of-plane distortion clearly dominates pincushion.

In Figure 4, we show individual representative fiber slit images at various locations on the focal plane. It can be seen that the spectrograph delivers sharp, clean images of the circular fiber slits across the whole focal plane. The images of circular slits are compressed along the dispersion direction by the anamorphic factor, and the resulting images are ellipses. The major axes of these ellipses are tilted with the direction perpendicular to dispersion, i.e., the spatial direction on the focal plane. This slit tilt is the result of a nonzero out-of-plane angle of incidence of most fibers (see Barnes 2004; Furesz 2008; Hearnshaw 2009). Slit tilt is zero on axis and increases with distance from the plane normal to the grating. On the blue side of the format, pincushion and color aberrations have opposite sign and almost cancel. On the red side, they have the same sign and reinforce each other. As a result, intrinsic slit tilt is increasingly amplified when moving from blue to red.

The slit tilt affects resolution, since extraction of spectral information is done along the rows and columns of the detector. As measured on full-resolution frames, the FWHM of spectral features varies by $\pm 10\%$, i.e., between 3.4 and 4.2 pixels. Accordingly, resolution changes along dispersion by a similar amount. However, since most stars exhibit nonzero broadening, the apparent fractional change is less, and thus the change in resolution is not as significant.

Other potential contributors to degradation of the slit image sharpness are intrinsic aberrations produced by the overall optical design, additional aberrations introduced by finite

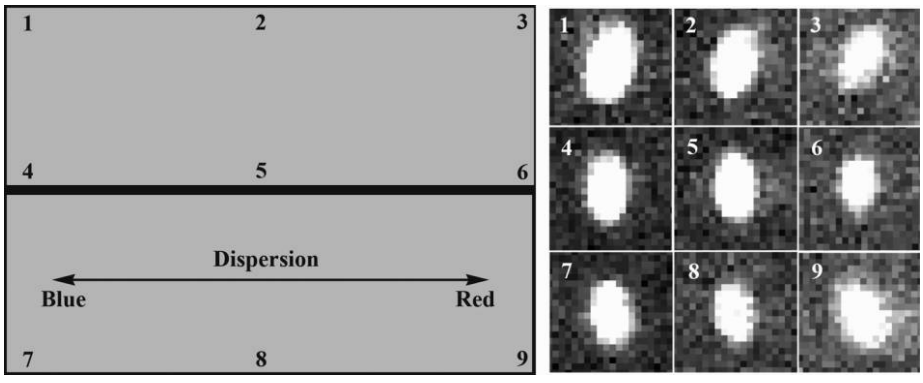

FIG. 4.—Slit images at various locations of the focal plane. *Left*: Schematic of focal plane showing location of slit images. *Right*: Corresponding slit images.

fabrication errors in the delivered optical elements, optical element misalignment, and variations in focus across the CCD format. Modeling the as-built optical system with ZEMAX demonstrates that the delivered point-spread function is smaller than 13.5 μm (1 pixel) over the entire focal plane. When added in quadrature to the overall resolution element dimensions ($\sim$4 pixels parallel to dispersion), the contribution of these errors is negligible. The effects of optical element misalignment and imperfect parfocalization across the CCD format are harder to assess, but experimentation with extrafocal images suggests that these effects are also negligible. The dominant contributor to the concentration of the slit images is the varying slit tilt discussed previously.

3.5. Optical Tuning Control

The spectrograph has three control axes that adjust focus and wavelength coverage. Orders redward of $\sim$5100 Å (order 32) overfill the CCD format (see Fig. 5).

The grating is mounted on a precise rotary stage, and so observers can tilt the grating to select red wavelengths that fall off the CCD format when the grating is operated on-blaze. This function is also useful to optimize positioning of extremely prominent features within certain orders (e.g., Hα or Na D) where a simple centering of the order may not be desirable.

The CCD cryostat is also mounted on a linear actuator for focusing the spectrograph. Since the order-separating filters do not all have the same optical thickness, the collimator is also on a linear focus stage to parfocalize the spectrograph in all filters.

3.6. Spectrograph Coatings and Fiber Feed Efficiency

The 250 μm core fibers that feed Hectochelle were purchased from Polymicro and drawn from a Hereaus-Amersil STU preform that transmits well from 0.37 to 1.8 μm, avoiding the blue cutoff of low-OH fibers and red absorption features present in high OH fibers. This preform was originally developed at the request of the Hectospec team. The intrinsic focal-ratio degradation in this fiber is very low: $\sim$95% of all the light transmitted by a 26 m length of fiber remains within an f/6 cone if the fiber is fed with an f/6 beam and care is taken to avoid stressing the fiber (Lu et al. 1998). Internal absorption in the 26 m fiber run is 6% at 6000 Å.

Since most of the refractive optics that constitute the Hectochelle are quite large, the choice of antireflection (AR) coatings was restricted to techniques that vendors could apply to large optics. For the AR coatings on the corrector lenses, only two vendors could supply competitive coatings. We selected a SolGel coating provided by Cleveland Crystals, Inc., mostly on the grounds of a risk analysis (Bohn & Leist 1998). Hard coatings are more durable than SolGel; however, an error in a hard-coating deposition would require full optical repolishing. SolGel coating proceeds in a two-step process—coating application, then hardening. After application, the coating is extremely soft and can be fully characterized before hardening. If the coating does not meet specifications, it simply wiped off and a new coating can then be applied. If the coating is acceptable, the SolGel is then hardened to increase its durability. The boost in transmission provided by SolGel coatings is spectacular, especially on the corrector fused-silica substrate material. Witness samples from the coating operations indicate transmission of 99% or better over the entire 3800–9000 Å Hectochelle passband.

The collimator mirror was coated at Lawrence Livermore National Laboratory with a proprietary, durable silver-metal oxide multilayer coating (Wolf & Thomas 1999). The coatings were optimized for the Hectochelle passband, having 96% reflectivity or better in 3800 Å to 9000 Å.

As was the case for the corrector lenses, the range of obtainable reflective coatings for the camera mirror was restricted by the capability of vendors to coat a meter-sized mirror. We selected Flabeg Corporation to deposit their front surface mirror protected aluminum mirror no. 756 on the camera mirror. This coating provided a 2–4% enhancement in reflectivity over a bare aluminum coating at most wavelengths in the Hectochelle passband.

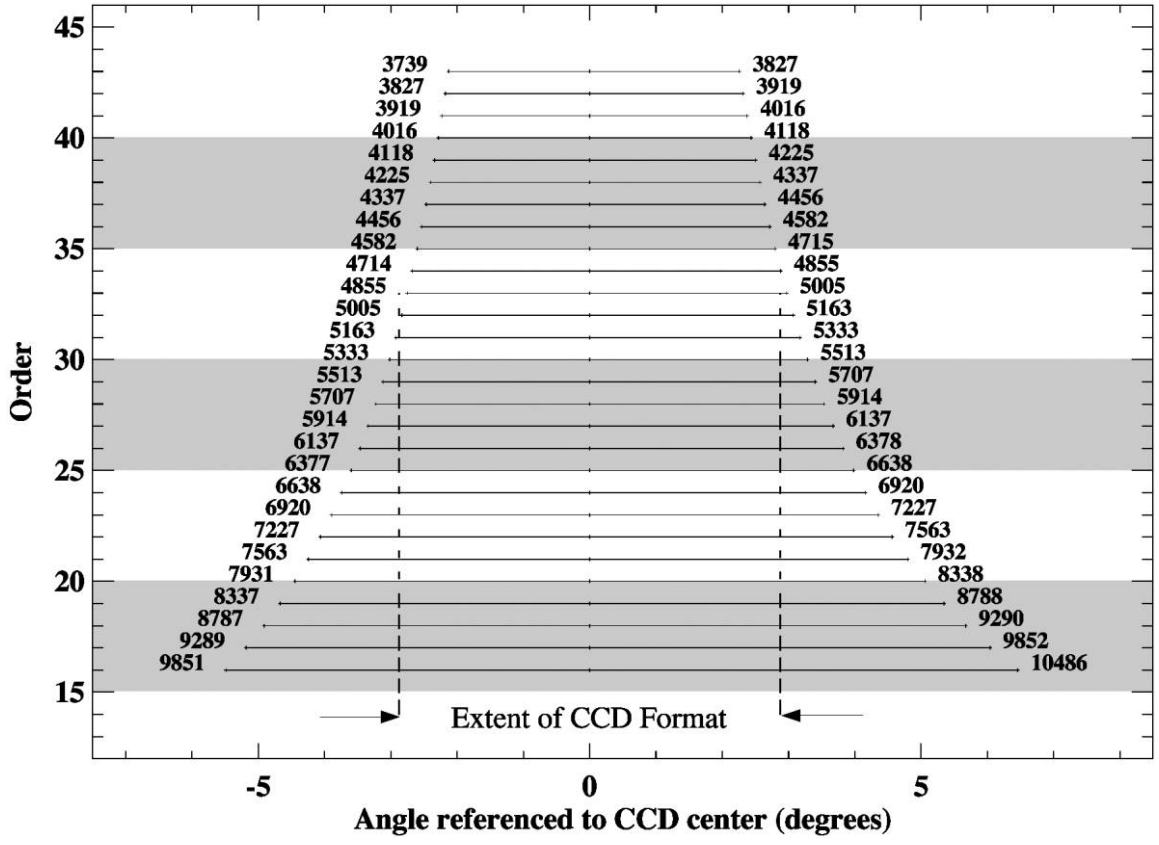

FIG. 5.—Echellegram of the Hectochelle indicating the passband of each diffractive order. Longward of order 32, the free spectral range is larger than the CCD format and some features fall off the focal plane.

Because SolGel has extremely high porosity, it has a potential to getter contaminants in the cryostat vacuum system and subsequently release those contaminant onto the focal plane during thermal or vacuum cycling. Since one side of the field flattener is in the cryostat vacuum, this optic was coated with a hard, broadband astronomy coating by Spectrum Thin Films, Inc. The performance of all these coatings is presented in Figure 6.

3.7. Optical Alignment

Final alignment was done entirely in situ (at the MMT) with a laser and alignment telescope mounted behind the camera mirror, which had a small hole at its vertex to allow visibility along the optical axis of the entire spectrograph. The laser was mounted at the start of alignment and provided a fixed absolute reference axis for all the optical elements. Since all the optics are spherical, alignment was accomplished by coregistering the reflected returns off individual surfaces to the outgoing beam. This process started with the camera and worked backward to the fiber feed. To coalign the two grating facets, two of the three grating tilt angles were set at zero order and the third angle was set with a Littrow return from the laser. Final alignment optimization was accomplished with a comparison between

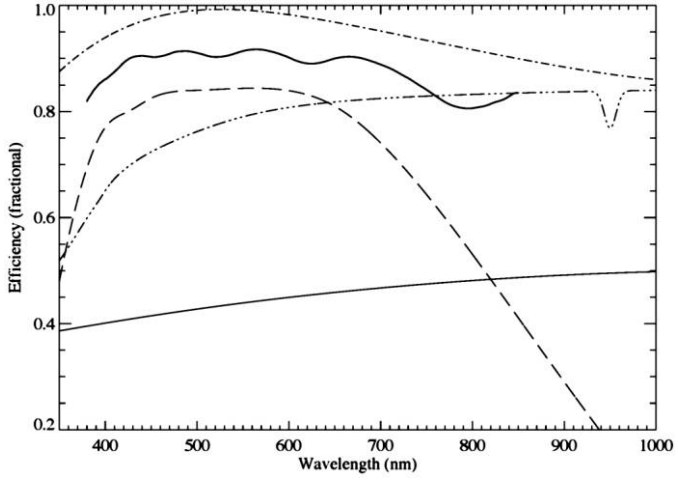

FIG. 6.—Measured efficiencies of various optical interfaces. The dot-dashed line is AR coating of all refractive optical surfaces. The top solid line is net reflectivity of collimator and camera mirror. The dashed line is CCD quantum efficiency. The triple-dot-dashed line is transmission through a 26 m length of optical fiber, from catalog values. The bottom solid line is grating efficiency averaged over a diffractive order. Filter transmission is not included.

focal-plane images across the entire focal plane (e.g., Fig. 4) and a detailed optical model written in ZEMAX, a ray-trace code developed by the ZEMAX Development Corporation.

3.8. Precision Radial Velocity Mode

An iodine vapor (I_2) cell, along with an unfilled "dummy" cell can be introduced into the spectrograph beam just in front of the fiber slit/shutter for precise radial velocity studies. In this operational mode, the filter changer is locked out. An RV31 (see the Appendix). filter is bonded to the I_2 cell. Currently, this operating mode must be set up manually.

4. MECHANICAL DESIGN

The mechanical design principles that guided the design of Hectochelle were to mount optics kinematically whenever possible and to athermalize all structures to minimize thermally induced flexure and relative displacements, as well as thermally induced stress in the large optics employed in the Hectochelle design. Whenever possible, the materials with the lowest obtainable coefficient of thermal expansion (CTE) were used, especially Invar and Zerodur. A more detailed discussion of our team's strategy for mounting large spectrograph optics can be found in Fata & Fabricant (1998).

4.1. The Hectochelle Thermal Operating Environment

The Hectochelle room at the MMT is on an outer wall of the MMT and could not be thermally controlled. Although Hectochelle is housed in a room-within-a-room, which provides some thermal insulation and stray light immunity, the room temperature must track the exterior ambient temperature so that the spectrograph room walls do not cause thermal convection in the MMT dome and compromise dome seeing. The room insulation damps out short-term thermal fluctuations, so temperature changes are gradual. While this mitigates thermal gradients, we endeavored to minimize thermal flexure in the presence of thermal gradients by design, to the greatest extent possible. Furthermore, all optical mountings were designed to survive $5\ g$ accelerations at a -5°C thermal soak to survive shipping loads. The maximal allowable stress coupled into any optic under these conditions was limited to 500 psi.

4.2. Optical Mounts

The camera and collimator mirror are both fabricated out of Zerodur. The collimator is only moderately concave, so the aspect ratio of the diameter to the vertex thickness is a conservative 10:1. The camera mirror presented something of a design challenge, since it is 1071.2 mm in diameter. The mass and cost of a Zerodur substrate large enough to apply a standard aspect ratio (diameter-to-vertex thickness) would have been problematic. However, the camera mirror is fast, so the optic has a deep bowl shape. As a result, the edge of the mirror is quite thick, regardless of the design vertex thickness. This geometry provides considerable rigidity. Detailed structural analysis revealed that an optic with 39.4 mm vertex thickness was structurally competent with a range of mounting schemes, despite a 27:1 diameter-vertex thickness aspect ratio.

Both mirrors are mounted in cylindrical cells with tangential flexures. Attachment to the mirrors is accomplished with circular Invar nubs bonded with Hysol 9313 epoxy filled with Siltex 44 silica powder. The silica is added to the epoxy to match the CTE of Zerodur as closely as possible. The silica-to-epoxy mix ratio is 4:5 silica by mass. The nubs are further azimuthally flexured to the tangential flexures to prevent coupling azimuthal moments into the optics.

The corrector lenses are quite large and require special attention to their mounting, especially the biconvex element, which has an extremely thin (17.8 mm) edge. The concaveconvex element has a relatively thick edge and is mounted with standard tangential flexures that are similar to those used for the mirrors. The optimal mount for the biconvex lens is a cantilevered tangential flexure (see Fig. 7). This mounting provides moment compliance around an axis tangent to the lens edge. The lenses are bonded to Invar nubs, also with silica-filled Hysol 9313 epoxy in the same 4:5 mass ratio.

The Hectochelle grating mosaic is 320 mm by 850 mm and is composed of two Richardson Grating Laboratory (RGL) 320 mm by 420 mm Zerodur grating facets. The grating substrates are 74 mm thick.

We initially explored the possibility of having RGL replicate two rulings onto a monolithic Zerodur substrate, as the UVES (Ultraviolet and Visual Echelle Spectrograph) team had (Dekker et al. 1994), but rejected this approach on cost grounds.

Having decided to meter the two individual facets mechanically, we did an extensive trade study comparing low-expansion alloy and low-expansion glass metering structures. This study led us to select Zerodur as the metering structure material. We originally envisioned fabricating the metering structure

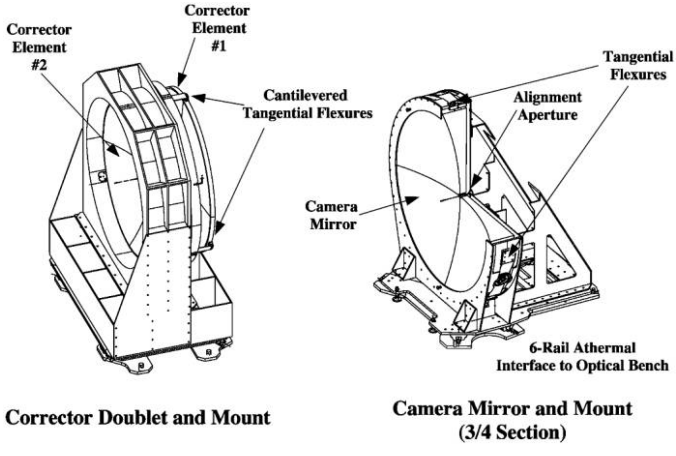

FIG. 7.—CAD drawings of the refractive corrector and camera mirror.

FIG. 8.—Hectochelle grating mosaic mounting. *Left*: fully assembled Hectochelle grating mosaic with the pupil mask removed. *Right*: Zerodur metering structure mounted on the rotary stage. Examples of the spring retractor and alignment micrometers are indicated. See the electronic edition of the *PASP* for a color version of this figure.

out of a monolithic Zerodur blank; however, cost considerations drove us to consider a bonded structure. At that time, the cost of a monolithic grating was 3 times that of individual facets. The metering structure Zerodur pieces are machined to shape and bonded by the Zygo Corporation (see Fig. 8). The adhesive used is Hysol EA 9313. In addition to the bonding, the metering structure pieces are also bolted together with inserts bonded into details machined in the Zerodur.

The mounting of the grating facets is fully kinematic. Axially, the grating facets are held in place by retractor springs attached to the metering structure that provide a tensile preload to pucks bonded on the back of the grating facets. A single lateral compressive preload meters both the facets against a fixed stop. Each facet is aligned with three axial micrometers and two vertical micrometers fixtured to details machined into the metering structure. Since the spectrograph is insensitive to alignment in the lateral direction, beyond simple registration to the spectrograph beam to avoid vignetting, no precision position metering features were needed in the lateral direction.

The metering structure is mounted on a precise rotary stage to permit adjustment of center wavelength of the various diffractive orders selected by the order-sorting filters. The rotary stage is a Newport model number RV350HA direct drive, annular rotation stage. It is encoded with 0.126″ resolution and achieves 0.72″ repeatability. It was controlled with a Newport model number MM4005 four-axis motion controller/driver, which communicated to the operations software through an RS-232-C interface.

The issue of CTE mismatch between the optical mounts and the optical bench was a matter of some concern. The optical mounts cause the bench Invar face sheets to pucker at low temperature if they were directly coupled. Since it was too costly to fabricate the optical mounts out of Invar, these were all fabricated out of mild steel. The only major mount component that was not fabricated specifically for Hectochelle was the precision rotary stage for the grating and the precision linear rails for the focus mechanisms. The rotary stage was chosen partially for its all-steel construction, which guaranteed that vertical thermal growth and shrinkage of the mounts would be homologous.

For many optical mounts, the CTE mismatch between the optical bench face sheets and the optical mounts was compensated with a system of three precision linear rails, purchased from THK, mounted to an Invar base that matched the optical bench CTE. The arrangement of this rail system is illustrated in Figure 9. The mount is fully radial compliant and hence completely athermal. Since growth and contraction of the mount is centered on each optic vertex, the optics that do not have linear focus mechanisms are all fixed in the horizontal plane. The two thin corrector lenses are mounted in the same structure. Since it was not possible to choose the center of the rail system to coincide with the center of either lens, we chose the center of motion to lie approximately halfway between the front and back nodal points of the lens system. Symmetry and load considerations for the optical bench/corrector lens mount interface led us to use a four-rail interface, rather than the three-rail geometry used in most other bench interfaces. The rails are arranged in an "X" pattern.

Because the mass of the camera mirror is quite high, an athermal six-rail system, rather than a typical three-rail system, is used to mount the camera mirror and mirror mount on the optical bench. The arrangement in this case is that of an asterisk (*), with the center of motion coinciding with the vertex of the mirror.

The collimator has a focus mechanism to parfocalize the different optical path lengths through the different order-sorting filters. The focus mechanism consists of precision THK linear rails, and the motion is actuated with stepper motors turning a precision lead screw.

4.3. Mechanisms

The robot and fiber feed system have been discussed extensively in Fabricant et al. (2005). Here, we repeat the salient

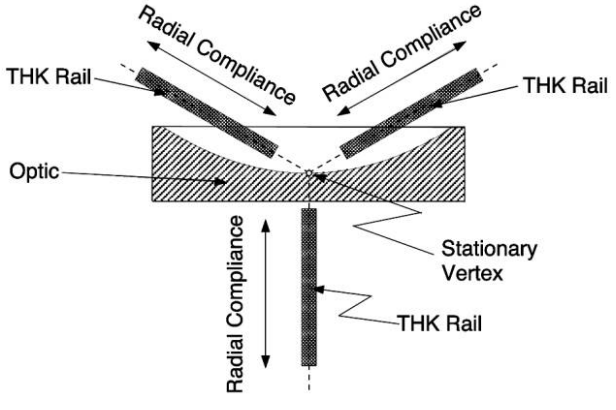

FIG. 9.—Athermal mounting system used for most Hectochelle optical mounts. Precision linear (THK) rails are mounted to an Invar base. The common vertex of the three rails is aligned with the horizontal location of each optic vertex.

features and those peculiar to Hectochelle. The fiber run that connects the Hectochelle and the robot positioner terminates, at the spectrograph end, in a fiber slit. Since the collimator has Schmidt geometry, the slit is curved and has a 1371.6 mm radius of curvature. The fiber shoe is the interface between the fiber run and the Hectochelle. The fiber shoe is held in place on the Hectochelle bench on the fiber shoe mount. The fiber shoe is moved *manually* between the Hectochelle and Hectospec, depending on which instrument is in use. This transfer is accomplished manually with a rail system that is mounted on the ceiling of Hectospec/chelle room and an off-loading system that is permanently attached to the fiber shoe. The off-loader is mechanically decoupled from the fiber shoe during observations, however, so that building vibration is not coupled into the spectrograph. The fiber shoe is mounted kinematically to the fiber shoe support, and positional repeatability of the mounting is ± 10 μm. The shutter is mounted integrally to the fiber shoe just in front of the fiber slit (see Fig 10) and *opens in 30 ms*. The optical train between the fiber input and the collimator introduces no vignetting.

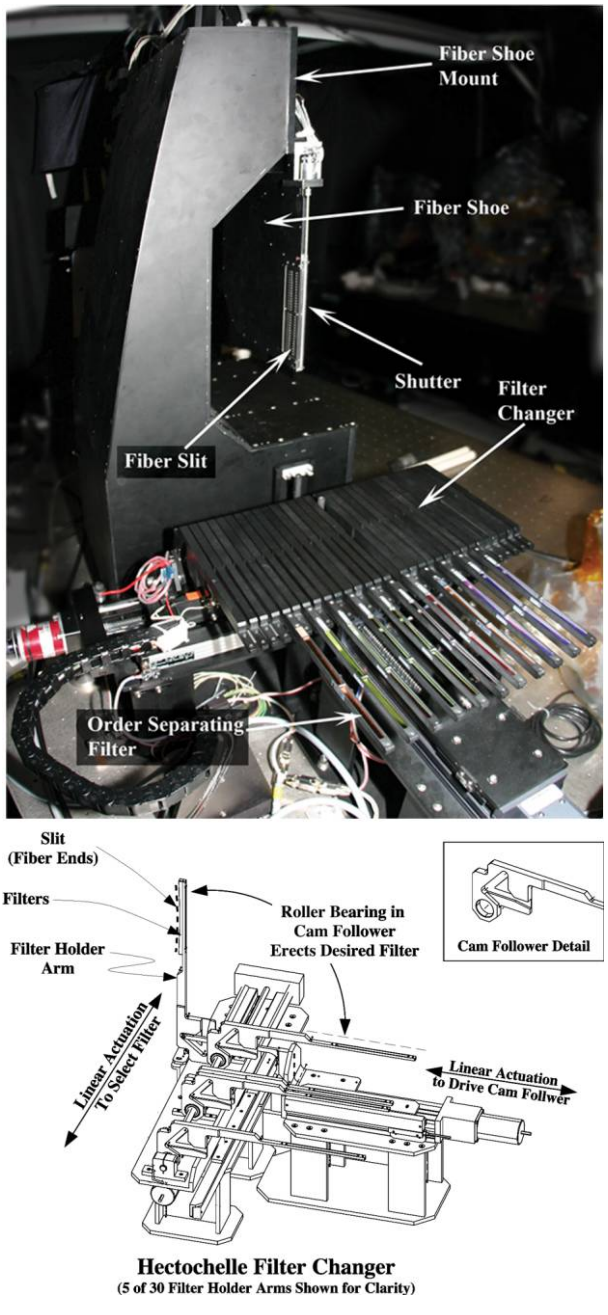

FIG. 10.—*Top*: Placement of the filter changer, the fiber feed/slit, and the shutter. *Bottom*: Operating principle of the filter changer cam-follower mechanism. See the electronic edition of the *PASP* for a color version of this figure.

The spectrograph shutter is mounted immediately in front of the fiber slit and is implemented as a rotating slotted cylinder (Fig. 11). The order-sorting filters are inserted directly in front of the shutter. Since the fiber slit, the fiber slit shoe, the shutter, and the order-sorting filters are in the parallel return beam of the collimator, every effort has been made to minimize the cross section of these components presented to the beam to minimized vignetting.

The filter changer is used to select the order-sorting filter and hence the passband of the Hectochelle for a given observation. It is positioned directly in front of the fiber shoe mount (see Figs. 1 and 10) The changer can potentially hold 29 filter pairs, but has only been populated with 11 filters since first light. Filters are

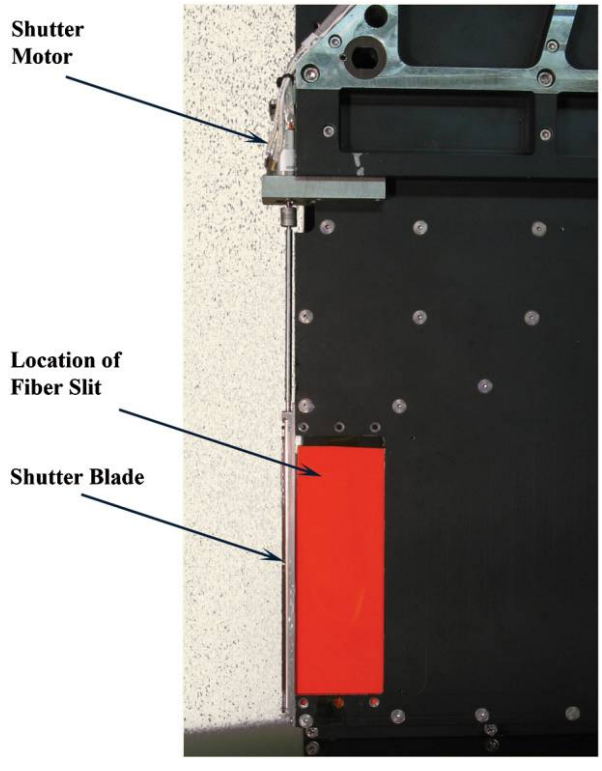

FIG. 11.—Location of the spectrograph shutter with respect to the fiber slit. See the electronic edition of the *PASP* for a color version of this figure.

selected by linearly translating the frame that holds the filters and the individual filters are erected in front of the shutter with a linear cam-follower mechanism. Since the filters are optical flats, no extreme precision is required of the mechanism other that alignment with the individual fiber beams, so actuation is accomplished with stepper motors. The order-separating filters are quite long, narrow and fragile, so they are held in Invar housings with Delrin pads and staked with RTV adhesive. Since the angle of incidence on the filters affects the passband, the each filter is tilted slightly to minimize the range of angles between the individual fiber beams (which lie on a circle) and the filters (which are flat).

4.4. Cryostat/CCD System Mechanical Design

Since the focal plane, and hence the cold head, is at an internal focus, the primary challenge in the design of the focal plane and cryostat was to minimize the cross section of the elements in the spectrograph beam to minimizing vignetting. The configuration we arrived at is shown in Figure 12. A single vane provides vertical support of the cold head. Lateral support of the cold vane is provided by the vacuum jacket of the cold finger. The cold finger is the conduction path between the cryogen reservoir and the CCDs. The vacuum-jacketed cold finger is a copper strap that is isolated from the jacket with small Kel-F buttons. The cryogen is liquid nitrogen, and the cryostat

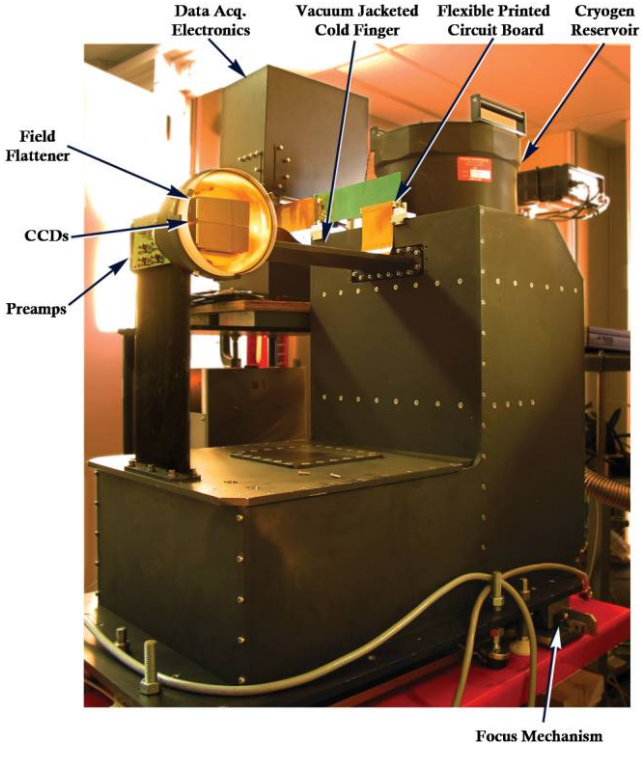

FIG. 12.—Hectochelle internal focus focal-plane cold head and associated hardware. See the electronic edition of the *PASP* for a color version of this figure.

reservoir was custom-designed by Infrared Laboratories. Its capacity is 10 liters, which provides a ~30 hr hold time between fills.

The entire cryostat system is mounted on precision linear rails, and so the spectrograph can be focused in response to thermal growth and shrinkage of the optical bench. The focus mechanism, like the collimator focus mechanism, is effected with a stepper motor through a precision lead screw.

The preamplifiers are mounted directly behind the cold head. This choice minimized the CCD-preamplifier wiring length to provide the best possible noise performance and not cause any additional vignetting. The electrical connection between the preamplifiers and the data acquisition system is made with a custom Kapton circuit board, which is very thin and flexible, thus minimizing the cross section presented to the spectrograph beam.

4.5. Optical Bench and Vibration Isolation

The optical bench was a custom design built in collaboration with the engineering department at Kinetic System. The face sheets are Invar 36, which are tapped with a standard pattern of $1/4 - 20$ threaded holes on $2''$ centers. The core is monolithic 5052 aluminum honeycomb to maximize conductivity between the Invar face sheets—thus minimizing thermal gradients. To further reduce the thermal gradient through the bench, the honeycomb was bonded directly to the face sheet, without a intermediate layer that is typically incorporated into optical bench designs to catch fluids or small part that fall in the holes. The bench was 5.49 m long by 1.68 m wide and 0.61 m thick. To reduce overall stack-up of the Hectochelle, eight cutouts in the bench for inset vibration-isolating supports were included in the design.

The MMT building, which houses the Hectochelle, rotates with the telescope azimuthal motion, so vibration isolation is essential. Hectochelle is mounted on eight vibration-isolating legs purchased from the TMC Corporation (model 16-26463-01). These isolators are operated in three control zones and actuated with a high-pressure, high-purity bottled nitrogen. The measured power spectra of the spectrograph room floor have modest resonances at 40, 60, and 80 Hz when the telescope building is rotating to track the telescope during observations. At these frequencies, the isolation system provides 40 dB or greater attenuation. There is no discernible difference between data taken when the building is static or in motion.

5. INSTRUMENT ELECTRONICS

5.1. CCD Controller/ Data Acquisition Electronics

The focal plane is a mosaic of two E2V 2048×4608 pixel backside-illuminated CCDs model CCD42-90 with 13.5 μm pixels. The data acquisition electronics are the same architecture as that used for all major CfA ground-based telescope instruments, including Hectospec, Megacam, and the MMT-Magellan

Infrared Spectrograph (MMIRS). The CCD controller was developed as a scalable design, which can be used to control CCDs, arrays of CCDs and infrared arrays with up to 72 video channels. It is based on the use of programmable gate arrays to generate all timing signals from a central crystal clock oscillator, with digital I/O and a fiber optic interface provided by a commercially available module. All boards of the system are 6U virtual machine environment (VME) format, plugging into a custom (non-VME) backplane that is optimized for very low noise electronics. Multioutput pixel rates in excess of 1 MHz are possible with this design, but in practice, readout speeds of 100–400 kHz pixel rate have been implemented for spectroscopic instrumentation due to CCD noise considerations. The entire CCD is read out in 60 s in unbinned mode at 100 kHz, which includes ancillary operations such as device clears before integration and communication handshakes between data acquisition subsystems. The design has proved to be robust in the field and produces CCD-limited 16-bit noise performance reliably. More details concerning this design can be found in Geary (2000).

In the case of Hectochelle, the system has unity gain and the readout noise is 2.7 e^- when read out at the customary 100 kHz pixel rate. Readout noise and gain have been measured directly with a ^{55}Fe k-band X-rays. Dark leakage current is extremely low -0.0001 e^- s^{-1} pixel^{-1} at the design operating temperature of -120°C. The background radiation rate is 1.5 events s^{-1} in the entire focal plane.

The focal-plane temperature is servoed with a thermistor/resistor pair mounted on the back of the plate that fixtures the CCDs. It was discovered during commissioning that even though this plate and the CCD structures themselves are fabricated out of Invar 36, the frequency of this servo loop required careful tuning to avoid motion of the focal plane due to thermal flexure of the CCD and the Invar mounting system.

5.2. Motion Control and Housekeeping

With the exception of the rotary stage for the echelle grating, all motion axes are actuated by stepper motors controlled with Nippon PCL-240MK motion controllers. These controllers are commanded through a Motorola 142 VME single-board computer running Linux. The rotary stage has an integral encoder. The filter changer has a linear encoder to position each selected filter with high precision so the cam-follower that erects the filter engages properly. All other control axes simply have limits defined by Hall sensors and positioning is metered as offsets from the limits. The collimator focus-stage actuation has an additional independent home sensor. Otherwise, home sensing is accomplished with the end-of-travel Hall sensors. Switching is accomplished with network-addressable power strip manufactured by Pulizzi Engineering, which was acquired by Eaton in 2007.

The optical bench has 16 thermistors bonded to both the top and bottom face sheets to monitor thermal gradients in the bench. All motors are also equipped with thermistors and continuously monitored to sense potentially hazardous overtemperature conditions.

6. THE THERMAL ENCLOSURE AND CRYOGEN HANDLING

As we have previously discussed, the Hectochelle is deployed in a room at the MMT between the outer wall and the telescope chamber, which essentially tracks outside temperatures. Before installation of the Hectospec and Hectochelle spectrographs, the room was refurbished and, to the greatest extent possible, insulated. Subsequently, a room-within-a-room was built primarily for light shielding, but a material was chosen to also increase the insulation of the spectrograph. The choice of material, driven largely by fire codes, was 2″ thick, 3 lb IsoFoam clad in 0.025 inch thick face sheets of black anodized 5005 series aluminum. This material is opaque to optical and infrared light, provides added insulation, is not very reflective, and meets the most stringent fire-code requirements. The structure, consisting of a vertical walls and a ceiling, increased the thermal time constant of the spectrograph room. The main conduction path into the spectrograph room is now through the floor, which is nearly impossible to insulate, given space constraints on the spectrographs.

We have measured the relationship between air temperature, bench face-sheet temperature, and, most importantly, shifts of wavelength on the instrument focal plane. A sample time series is plotted in Figure 13 for a single CCD. The correlation between shifts of the wavelength on the CCDs is evident. Modest temperature fluctuations (~1°C) can produce macroscopic (1/2 pixel) shifts. For reference, a half-pixel shift at 5200 Å corresponds to approximately a 1 km s^{-1} velocity shift. For comparison, the Poisson-limited Doppler precision (PLDP; Connes 1985) of which Hectochelle is capable is 25–50 m s^{-1} with the S/N obtained in a 1 hr exposure on a 15th magnitude star. A good calibration protocol is essential to remove thermal shifts of the wavelength scale if Hectochelle is to achieve its full scientific potential.

The dramatic thermal spikes in Figure 13 are the result of spectrograph cryostat fillings with liquid nitrogen. Bulk cryogen is stored in a large dewar external to the spectrograph room and is delivered through vacuum-jacketed, stainless steel cryogen feed lines. These lines provide an extremely high level of insulation; however, joinery at the spectrograph cryostat is an inevitable source of thermal leakage. Since the data in Figure 13 were taken, we have improved the insulation and immunity temperature fluctuations caused by cryogen fills. The data we present are chosen to illustrate a number of thermal effects. In particular, the temperature spikes associated with cryogen fill produce thermal distortions along the dispersion direction, while ambient temperature changes induce a large shift perpendicular to the dispersion direction—i.e., in the spatial direction. This is understandable in terms of the spectrograph bench

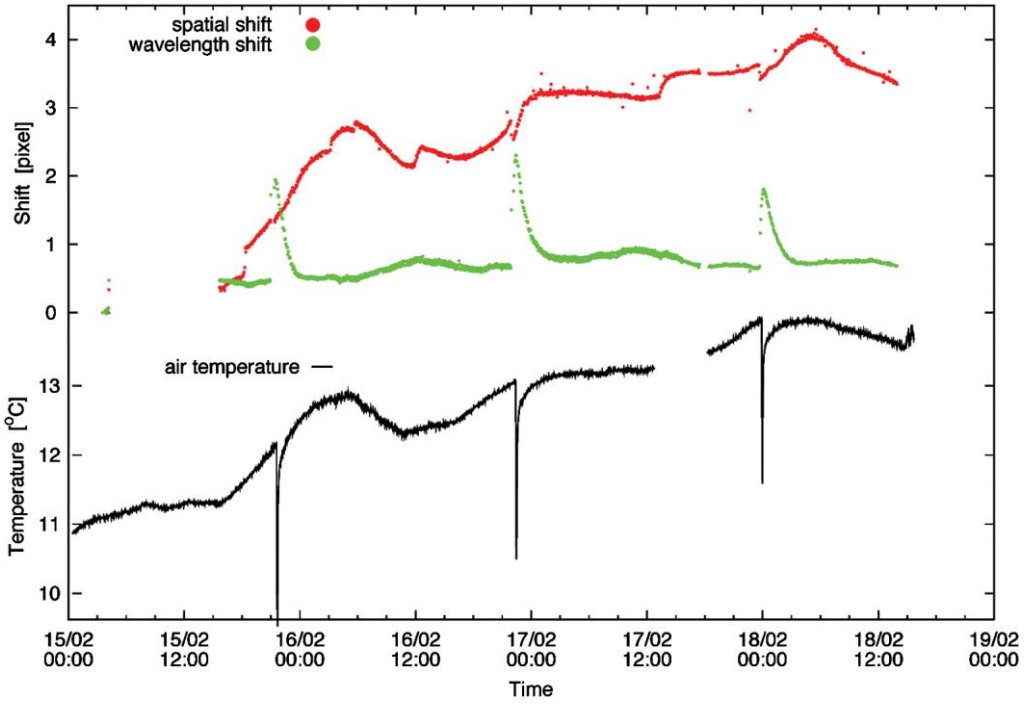

FIG. 13.—Thermal history of spectrograph room air temperature and mechanical shifts of the Hectochelle focal plane parallel and perpendicular to the dispersion direction of the spectrograph. See the electronic edition of the *PASP* for a color version of this figure.

geometry, which is long and narrow. Gradients through the bench will cause it to curl more severely along it longer dimension, which will produce up/down motion of the echellegram, which is parallel to the spatial direction. The spiked motion of the echellegram parallel to the dispersion direction in the lateral direction is probably due to local gradients in the focal-plane mounting and the cold head itself, introduced during cryogen fills. The relaxation time for the fill-related spikes is 4–6 hr. If the dewar is always filled in the morning, immediately after observations are complete, this is not an issue for wavelength stability.

7. SOFTWARE

A sophisticated fiber configuration planning computer program, xfitfibs, has been developed at CfA to optimize the arrangement of the optical fiber buttons on the robot focal plane. This has been discussed in relation to Hectospec operations in Fabricant et al. (2005). The algorithmic basis for xfitfibs is presented in Roll et al. (1998).

SPICE, the Hectochelle observing software suite, is a Tcl/Tk program that provides a graphical user interface to the Hectochelle. SPICE follows the protocols of ICE, a data acquisition system developed for MMT instrumentation (Conroy et al. 1998). The look and feel of SPICE is the same for all the operations software developed by the CfA Optical and Infrared Ground-Based Instrumentation Group. Many of the features of SPICE have been discussed in Fabricant et al. (2005) in the context of Hectospec operations; however, Hectochelle is a significantly more complicated instrument, supporting a larger variety of operating modes. For this reason, the Hectochelle SPICE version has many additional features.

The SPICE GUI panels are shown in Figure 14. The left panel—the exposure status window—informs the observer of all the relevant parameters of an individual exposure. The right panel—the SPICE window—is divided into two halves. The upper half reports the status of the spectrograph, while the software buttons that effect control of the spectrograph—stop, pause, abort exposures, change order-sorting filter, or select observing mode—are located in the lower half of the panel. The status of settings and actions is colored-coded. Green indicates an "on" state or readiness to start a new operation. Yellow indicates a process in progress or in an intermediate state. Red indicates an "off" state or a malfunction/trouble. Tabs along the centerline of the SPICE window organize the various functions and phases of Hectochelle operations, e.g., startup operations, standard observing functions, and specialized observing modes and functions.

Many setup functions are preselected by SPICE and are not accessible to nonengineering observers. While it is standard procedure to focus the spectrograph in one order-sorting filter at the start of the night, parfocalization of the collimator and camera for all other filters is fully automated. The echelle grating is, in general, operated slightly off-blaze to match the filter passbands and optimize the location of prominent spectral

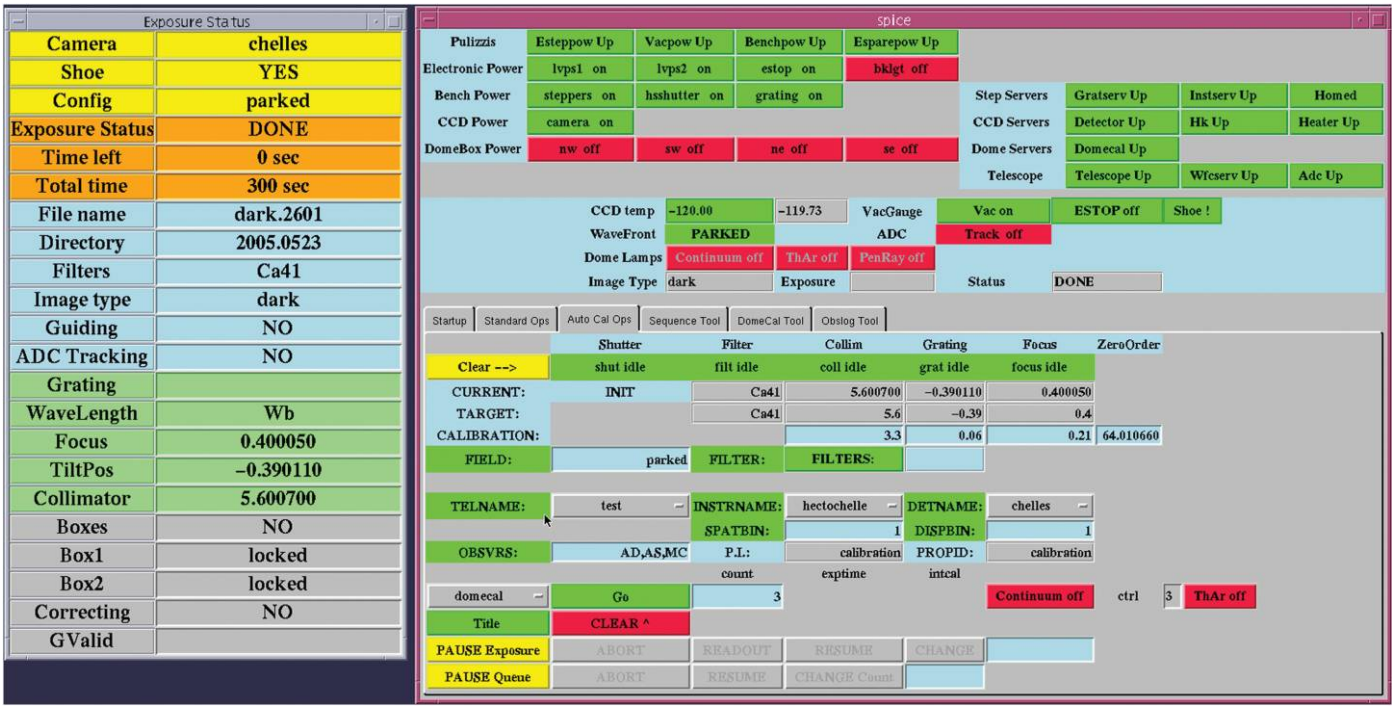

FIG. 14.—SPICE standard observing window. See the electronic edition of the *PASP* for a color version of this figure.

features on the CCD format (e.g., Na D, Hα, etc.). SPICE automatically sets the tilt of the grating when the order-sorting filter is changed.

SPICE offers the observer the possibility to take a wide variety of exposures—bias, wavelength-scale calibration with thorium-argon lamps, astronomical object observation, etc. For each mode, there is detailed checking of the spectrograph configuration prior to the initiation of an integration to guarantee that all the parameters and settings are consistent with the observing mode, e.g., that the incandescent lamp is on for a dome flat and off for a science object exposure. These parameters can generally be overridden when an override does not lead to a nonsensical or dangerous configuration.

All the mechanical parameters of the exposure are set through SPICE, e.g., turning calibration lamps on and off, exposure duration, detector binning, etc. Sequences of primitive operations can be scripted with the Sequence Tool tab in the SPICE window.

Further details concerning the SPICE software can be found in Szentgyorgyi et al. (2006).

A description of the robot positioner software can be found in Fabricant et al. (2005).

8. CALIBRATION SYSTEM

A nettlesome problem with high-dispersion multiobject spectrographs is that of wavelength calibration. Hollow-cathode lamps with high atomic number cathodes—usually thorium, the wavelength reference of choice—are intrinsically weak emitters. The canonical technique of bouncing calibration lamp light off a quasi-Lambertian dome reflector, accepted as a reasonable proxy for a source at infinite conjugate, delivers very low light levels into the optical fibers feeding the spectrograph. An experiment with a green laser at 5320 Å showed that the attenuation between a light source and the Hectochelle focal plane was a factor of 10^{-13}. This is not an issue for fixed-configuration fiber instruments, where calibration light can be injected into the fiber feed. No such convenient opportunity exists in an instrument where the fiber slits are reconfigured between observations. Other multiobject echelle spectrographs have generally solved this problem in equally ad hoc ways or at the expense of considerable added instrumental complexity. Giraffe avoids configuration-dependent wavelength-scale variations by mounting a wavelength calibrator on the fiber positioner head and illuminating fibers individually; however, this is time-consuming, and Giraffe only calibrates a subset of fibers in this way to track shifts of the wavelength solution. Low-dispersion spectrographs do not require a high density of emission features and can be calibrated with brighter gas emission lamps (e.g., He, Ne, and Ar). The faintness of thorium lamp emission, especially when reflected off a dome screen, results in very long wavelength calibration exposures that have low S/N. The duration of these exposures (20–60 minutes) is unacceptably long for interobservation calibrations during the night. On the other hand, thermal shifts on hour timescales make it necessary to calibrate at a 1 hr cadence if acceptable radial velocity precision is to be obtained.

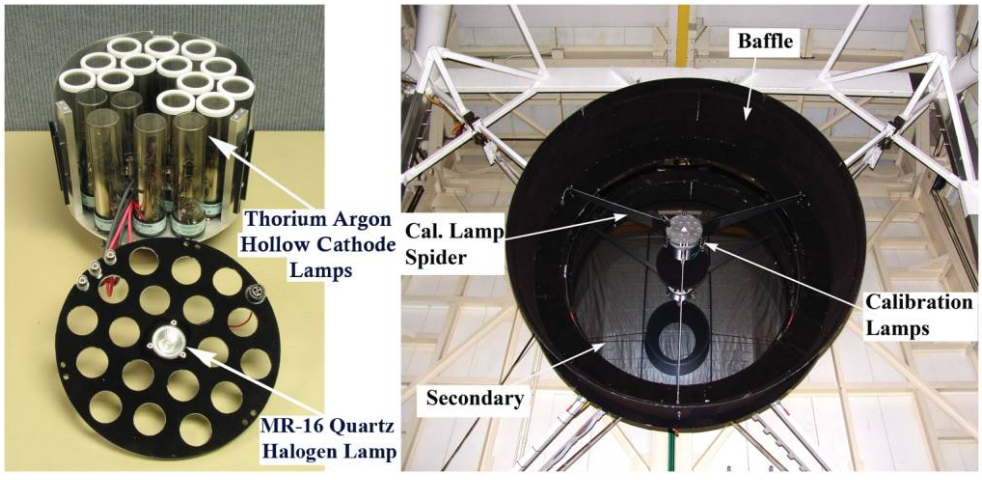

FIG. 15.—*Left*: Cluster of 18 thorium-argon hollow-cathode lamps and the quartz-halogen incandescent bulb. *Right*: Mounting of the lamps just in front of the MMT secondary mirror. See the electronic edition of the *PASP* for a color version of this figure.

Although other calibrators exist for wavelength-scale calibration, e.g., iodine vapor cells, they are all for specialized applications in limited wavelength intervals and are not useful for general-purpose calibration of high-dispersion astronomical spectra.

Our solution to this dilemma is to mount a cluster of 18 thorium-argon hollow-cathode lamps directly in front of the telescope secondary, pointing directly at the focal plane and the optical fiber ends (see Fig. 15). This approach improves the coupling of light into the fiber by a factor of 8 and calibration spectra with a typical S/N of 40 in 5 minutes.

The drawback to this technique is that the mounting of the lamps is not at the exit pupil of the telescope. The geometry of the curved robot positioner focal plane is extremely telecentric, so the angle light from the calibration lamps at this location enters a fiber depends on the position of the fiber in the focal plane. This in turn affects the pupil illumination of the spectrograph, which alters the wavelength scale subtly. The net effect is that calibration scale is slightly dependent on fiber configuration and we do not reach the PLDP of which Hectochelle is capable. At present, we have demonstrated the ability to achieve 100 m s^{-1} radial velocity measurement repeatability in high-S/N solar spectra over several-month baselines. Hectochelle should reach a PLDP that is 3 times more precise.

We have been experimenting with tunable laser calibrators, which are bright enough to reflect off the MMT dome screen and to achieve the PLDP limit. Tunable laser calibrators have the additional advantage that they can produce wavelength fiducials at arbitrary spatial density. Furthermore, at the red end of the optical spectrum, argon-filled hollow-cathode lamps have extremely bright argon emission features, which are not good calibrators, but they saturate the detector badly and produce high-level stray light, ghost images, and fringing patterns in the focal plane. This calibration system is still in prototype phase, and some additional development is required to produce a general-purpose calibrator that can be operated routinely (Szentgyorgyi et al. 2008; Cramer et al. 2009).

The thorium-argon hub also has an incandescent continuum lamp—a MR-16 quartz-halogen bulb—which is used for tracing apertures on the focal plane, throughput correction and correction of pixel-to-pixel variations. This lamp is considerably easier to use than the facility dome lamp system that reflects off the dome, as the dome screen is mounted on the telescope enclosure slit, and the slit itself must be closed to deploy the dome screen. Opening and closing the slit throughout the night is operationally complicated and takes up valuable observing time. However, the flat-field images the hub incandescent lamp produces are inferior to those taken with a facility lamp boxes mounted the dome screen for fringe removal in red-order spectra and determining throughput corrections. The fringe pattern depends critically on spectrograph pupil illumination, which is configuration-dependent when using the hub incandescent. For the purpose of tracking shifts in the aperture-tracing template throughout the night, however, the incandescent lamp in the hub is more than adequate.

9. OPERATIONS

All Hectospec and Hectochelle observations are queue scheduled. A queue observer operates the spectrograph. Queue observers are drawn from the observational teams that have been allocated time on Hectochelle in a given trimester. The robot positioner is run by a professional observer who is experienced in robot operations.

Science teams are required to submit their fiber configurations several weeks in advance of potential observations. Fiber configurations are reviewed by a CfA instrument scientist to guarantee goodness of guide star selection and the adequacy of the astrometry. Successful target acquisition with the robot

TABLE 3
TYPICAL DATA PRODUCTS COLLECTED IN HECTOCHELLE OBSERVING NIGHT

Data type	Number of exposures	Cadence	Duration/exposure
Bias	10	Daily	0 s
Dark	10/binning mode	Archival	1200 s
Dome contin. flat	10/binning mode and filter	Dawn and dusk	5–20 s
Deep ThAr	5/binning mode and filter	Dawn and dusk	200–700 s
Twilight sky	2–4/binning mode and filter	Dawn and dusk	Variable
Science obs.	3/configuration and filter	Through night	1200–3600 s
Interobs. ThAr	2/science observation	1/hr	120 s
Interobs. contin.	1/science observation	1/hr	4 s

positioner requires 0.2–0.3″ relative astrometry. The instrument scientist prepares a queue schedule for each run. The schedule is revised every day during the run to attempt to equilibrate the observing time among the various approved programs. Unlike other queue systems, queue scheduling is not prioritized in any way, e.g., on time allocation committee grades. Exposure-time thresholds, critical duration, phasing, and cadence of observation are taken into account when a night's observations are scheduled.

On any given night, the robot operator assesses the observability and suitability with respect to seeing, sky clarity, and moon position. The actual observing schedule is then determined dynamically in consultation with the queue observers in response to changing sky condition and current moon position.

At the start of each evening, the queue observer or robot operator focuses the spectrograph. Even though the face-sheet material of the Hectochelle optical bench has an extremely low coefficient of thermal expansion, when the ambient temperature changes significantly from night to night, refocus is sometimes needed. This is accomplished automatically with a script that collects a sequence of extrafocal images on either side of the focus and determines the location of the minimum spot size averaged over the whole CCD format.

A full calibration sequence is taken for every observing mode anticipated on a given night, i.e., all requested order-sorting filters and binning modes. Since the acquisition of calibration products can take a long time, the number of modes permitted in a given night is limited and this may affect the observing queue.

The Hectochelle is operated with a deployable wavefront sensor that is used to correct the figure of the MMT primary mirror between exposures. Wavefront sensing and figure correction are generally repeated whenever the telescope is moved to a new field.

Calibration products (see Table 3) generally include multiple bias, dark, continuum flat, twilight wavelength scale and thorium-argon wavelength-scale frames. Thorium-argon wavelength-scale exposures are repeated throughout the night at approximately a 1 hr cadence. Since typical science exposures are 15–20 minutes long, this corresponds to taking a calibration exposure at the beginning and end of a sequence of three science exposures. A deep set of continuum flats is taken at dusk with the dome lamp system for throughput correction and fringe removal. Continuum flats using the hub mounted incandescent bulb are taken throughout the night for each new fiber setting to track aperture drift in the spectrograph. Most calibration data are collected again at dawn, when possible.

The Hectochelle and Robot positioner are extremely time-efficient instruments and have very low operating costs when compared with other instruments. A typical observing sequence is presented in Table 4. The operational overhead to change a configuration is under 20 minutes (again, see Table 4) Individual configurations are then typically observed for 1–4 hr.

Special observing protocols occasionally require additional steps in the observing preparation process; e.g., when observing bright stars it is necessary to nod the telescope away from the stars so that the stellar spectra are not imprinted on the calibration frames.

For the very best sky subtraction, ideally, sky data must be taken with the same fiber and in the same configuration as the science object, with the same exposure time. Thus, for these purposes, the telescope is also nodded and a sky exposure is made without changing the fiber configuration. These exposures should have the same duration and be as contemporaneous as possible. There are several reasons for this. Fiber-to-fiber throughput correction is not perfect and changes over time.

TABLE 4
OPERATIONAL OVERHEAD TIMES FOR HECTOCHELLE SETUP

Operation	Execution time
Slew to zenith to configure fibers	1 minute
Configure fibers	5 minute
Slew to target	1 minute
Wavefront sense/adjust primary	5 minute
Acquire guide star	2 minute
Flat and wavelength calibtration	5 minute
Total overhead	19 minute

There are also significant spatial and temporal variations of sky conditions.

In practice, we have adopted the following two protocols to perform sky subtraction: one is an offset sky exposure, and the other is by means of dedicated sky fibers allocated among the fibers not positioned on science targets. The offset sky exposure is done by nodding the telescope off the target field by a few arcseconds, while preserving the fibers in the exact same configuration. Ideally, the sky exposure should have the same integration time, but this is a time-consuming process. However, when sky background is changing over short spatial scales, e.g., an embedded stellar cluster such as NGC 2264, nodding is required background subtraction.

In the case of dedicated sky-sampling fibers, the fiber configuration code assigns apertures to evenly cover sky areas across the field of view. Arrangement of sky fibers can be also optimized so that they are placed closer to science targets than would be achieved with a more uniform coverage. These spectra are then averaged after extraction, and a "master" sky is subtracted from each aperture. During the averaging process, account is taken of where the sky fiber was placed in the field, since the actual angular sky coverage is dependent on the distance from the center of the field. The averaging and subtraction of the sky have to be done after the spectra are corrected for throughput variations, which is done based on a flat-field image. Typically, a single sky spectrum has a S/N of 6–8 per resolution element in a 15 minute exposure. When the averaged "master" sky is subtracted from individual sky spectra, the subtracted spectrum is quite flat, with a dispersion that is less than 1.5 times the readout noise. In our experience, stellar spectra with S/N twice the sky level can be corrected adequately for sky background.

To protect data from accidental erasure, a copy of every data file is immediately written to an access control hard disk on site and mirrored to an archive at CfA. Observers are automatically sent e-mails with the location of their data and necessary calibration on the CfA archive. Access to the archives is controlled so observers only have access to their own data. The data are sent directly into a reduction pipeline, and the results are reviewed daily to detect anomalies. Observers are informed of any problems in the data quality before the next night of observing commences.

The primary performance parameters of a spectrograph are throughput and resolution. The properties of the point-spread function and slit image have been discussed in § 2. The spectrograph focuses to specification in all orders for which we have order-sorting filters, which nearly span entire the usable passband of the Hectochelle.

10. INSTRUMENT PERFORMANCE AND DATA REDUCTION

The nominal resolution of the spectrograph is 32,000 at 5200 Å, if the resolution is taken to be the simple diameter of the circular fiber slit (i.e., optical fiber) image. Projection of the circular slit image onto the dispersion axis effectively boosts this resolution by a factor of 1.46. Because the Hectochelle is anamorphic, the slit images are elliptical. Mild pincushion distortion and out-of-plane angles of incidence on the grating tilt the major axis of the elliptical slit image, which is seen in Figure 4 to vary along both the dispersion and spatial axes of the focal plane. These effects reduce the boost factor somewhat. A typical resolution of 38,000 is achieved.

The predicted and achieved efficiency are presented in Figure 16. The predicted efficiency does not include the blaze function of the grating, so it should define the envelope of the blaze peak of the measured efficiency. Figure 16 shows the agreement between the prediction and data in order 37. The agreement is not as good in order 25 and even worse at order 31. This is explained in large part by the fact the echelle is grating is operated significantly off-blaze in the discrepant orders to optimize the location of important spectral features on the CCD format and match the delivered passband of the order-sorting filters. Using the formalism of Bottema (1980), we estimate the loss at peak throughput in these off-blaze configurations to be 10–12%. This explains the performance well. In order 31, we suspect that we have slightly overestimated the transmission of the SolGel antireflection at peak (see Fig. 6), which coincides with the center of order 31. Since there are 14 SolGel coated air-glass interfaces, when the field corrector and ADC prisms are included, a discrepancy of under 1% in the individual coating transmission could produce the difference between the calculated and measured throughput for the system as a whole. This hypothesis is supported by the fact that of all

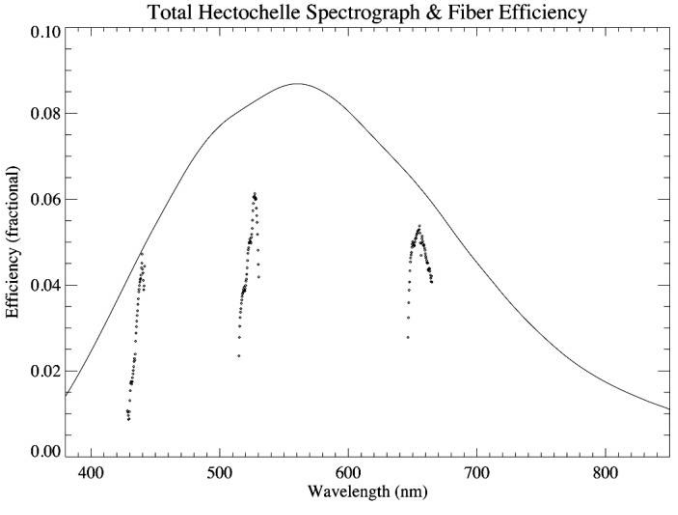

FIG. 16.—Total spectrograph efficiency as a function of wavelength. Solid curve is combination of all losses in Fig. 6, but using peak grating efficiency. Small triangles are measured throughput values, which include telescope and slit losses, internal order-sorting filter transmission, and the grating blaze function. They are (*left to right)* orders 37, 31, and 25.

the performance curves in Figure 6, only the SolGel curve is peaked near 5200 Å.

The CfA Telescope Data Center has written a data reduction pipeline that can produce wavelength-calibrated, one-dimensional spectra from raw Hectochelle data and calibration frames. The pipeline consists of a series of shell scripts that largely call the standard IRAF[1] routine for CCD processing, aperture tracing, aperture extraction, and wavelength calibration. In particular, the numerous routines in the IRAF APEXTRACT package are used to produce the individual one-dimensional spectrum and then wavelength calibrate them. As we previously mentioned, the best sky subtraction is obtained by nodding the telescope slightly to a position where the science objects no longer fall on the fiber ends and taking an exposure of the night sky through the science object fiber with the fiber in their science configuration. Since this procedure requires that the sky exposure duration be the same as the science exposure, this is observationally onerous and only adopted when the best sky subtraction is required. A more common procedure is to have xfitfibs allocate all the fibers that are not used for science objects to sky subtraction. Typical science configurations leave 30–60 sky fibers, which sample the field of view relatively uniformly and quite densely. The pipeline also corrects a number of systematic effects, e.g., the radial dependence of the effective fiber-collecting area due to mild distortion of the corrected telescope optical train.

11. EXAMPLES OF HECTOCHELLE SCIENCE PROGRAMS

Hectochelle is particularly powerful for studies relatively high spatial density aggregations of similar objects on the sky. It has been prominently used for studies of globular clusters, open clusters, Local Group dwarf spheroidal galaxies, and nearby galaxies in general.

One of the first surveys, as part of the commissioning, targeted nearby star-forming regions. A study of NGC 2264 was performed by Furesz et al. (2006) to investigate the inner radial velocity structure of the stellar component in the cone-nebula complex. NGC 2264 is a young cluster at a distance of 800 pc. A total of 1078 stars were observed, drawn from a target list of 1563 stars in the $40 \times 60'$ field (see Fig. 17). The data were collected in five fiber positioner settings over three nights. Each setting was observed in three or four exposures, each 15 minutes in duration. Since stellar Hα emission from the ongoing accretion can help in confirming membership, the observations were done with the OB25 order-sorting filter, which is centered on Hα. The Ca and Fe features covered by the same spectral order provided radial velocity information to determine membership for stars past their T-Tauri phase. For stars with J magnitudes in the $10 < J < 13$ range, Hectochelle achieved a S/N yielding a radial velocity precision of better than 1 km s^{-1} for almost all stars, which was sufficient to identify kinematically distinguished subgroups within the cluster.

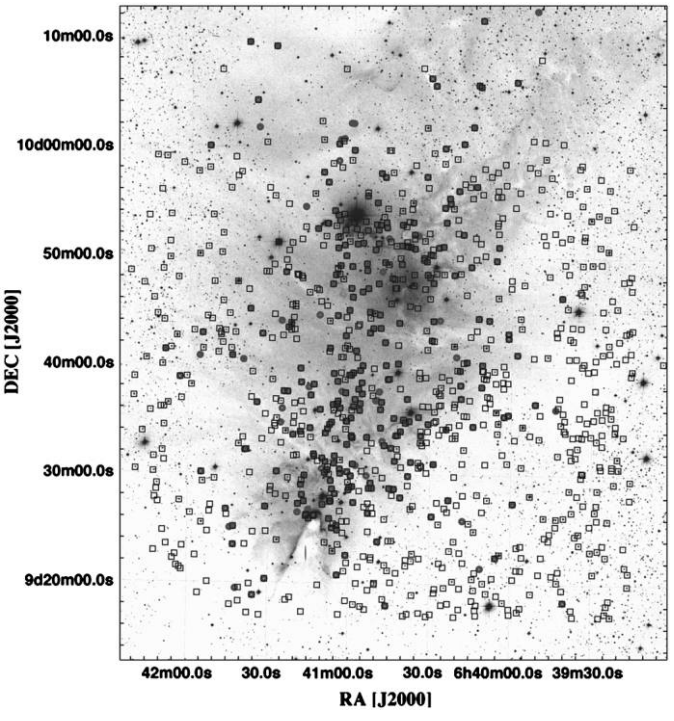

FIG. 17.—Stars observed in NGC 2264 with Hectochelle. Open squares indicate observed stars (from Furesz et al. 2006).

Another measure of Hectochelle performance can be illustrated by plotting R magnitude versus the S/N of spectral cross-correlation with template stars (R) (see Fig. 18). Since these stars were only observed once in most cases, the scatter in Figure 18 is to be expected, as many stars are binary or noisy. Nonetheless, the upper envelope of the scatter plot is indicative of the R that Hectochelle delivers in 3×15 minute observations of quiet, solitary stars.

As a whole, the cone-nebula association turned out to exhibit an unusually broad, non-Gaussian radial velocity distribution that has a ~3.5 km s^{-1} dispersion. This and the spatial/radial velocity structures discovered in these investigations clearly show that this young cluster is not relaxed. The results of this survey have been used to sort among competing models of cluster formation and dynamics. These data were subsequently reanalyzed by Baxter et al. (2009) to revise the distance and age of NGC 2264 exploiting rotation measures of 97 stars in the Furesz et al. sample.

Hectochelle has been used for studies of internal dynamics of Local Group dwarf spheroidal galaxies. In a study of Leo I, 108 RGB cluster members were observed in seven fiber configurations covering a $20 \times 33'$ field (Mateo et al. 2008). Each

[1]IRAF is distributed by the National Optical Astronomy Observatories, which are operated by the Association of Universities for Research in Astronomy, Inc., under cooperative agreement with the National Science Foundation.

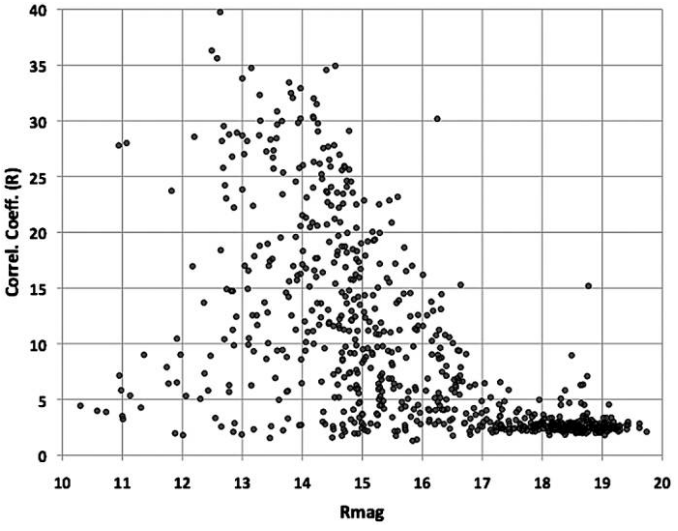

FIG. 18.—Relationship between R magnitude and the autocorrelation coefficient (R) obtained for stars is the NGC 2264 survey.

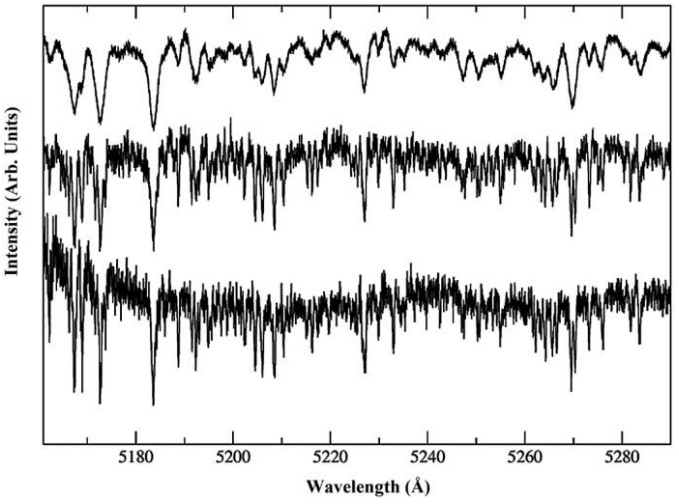

FIG. 19.—Three M31 globular clusters with very different internal velocity dispersions (from top to bottom, 27.0, 7.7, and 5.8 km/s). The spectra were Gaussian-smoothed with a σ of 1 pixel. The strongest lines are those of the Mgb triplet near 5180 Å.

field was observed in three 1 hr integrations. Observations were made using the RV31 radial velocity filter, which includes Mg I/Mgb features near 5200 Å. The target stars had V magnitudes between 20.9 and 17. Rather remarkably, the mean radial velocity error (1σ) was 2.4 km s^{-1} with a systematic error of <1 km s^{-1}. Data obtained for a similar study by were used to determine the mean metallicity of Leo V (Walker et al. 2009), observing RGB stars in the magnitude range of $21 < r < 19.5$. They determine the metallicity of these weakly lined stars ([Fe/H] $= -2$) with a remarkable standard deviation of 10%.

Another Hectochelle project that is currently in progress seeks to measure the mass-to-light ratios of M31 globular clusters by measuring their internal velocity dispersions (Strader & Caldwell 2011, in preparation). Shown in Figure 19 are three M31 globular clusters, with very different internal velocity dispersions (from top to bottom, 27.0, 7.7 and 5.8 km s^{-1}). The RV31 filter was used to obtain these data, with a combined exposure time of 3 hr. This project has increased the number of clusters with measured dispersions from 27 to more than 100 with just 6 hr of observations.

Hectochelle is being widely used to study the dynamics of chromospheres in globular cluster stars to search for signatures of mass outflow and stellar winds. Filters of interest are usually OB25, which contains the Hα line at 6563 Å, and the Ca41, which contains not only the Ca II resonance H and K lines, but Hε of the Balmer series. Examples of these spectra of red giant stars in the globular clusters M13 and M15 are shown in Figs. 20 and 21.

The Hα line typically has a deep core and emission wings arising in a stellar chromosphere. The asymmetry of the core and the emission wings and the wavelength shift of the core with respect to the nearby photospheric absorption features reveal dynamics in the low chromosphere. After normalizing the spectrum to the continuum, these characteristics of the line profile can be measured. In this case, the wavelength standards were determined by ThAr lamp exposures, which led to a systematic stretching of the wavelength scale over about ~20 Å, depending on aperture. The amplitude of this variation is ~2 km s^{-1} and can be removed.

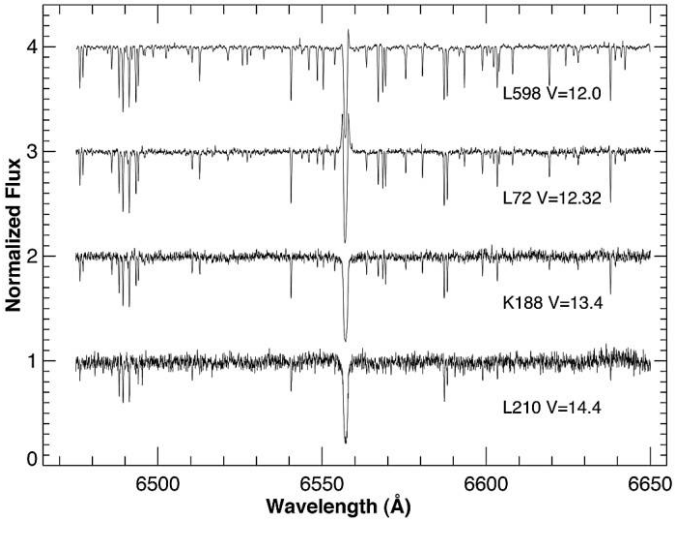

FIG. 20.—Hα region of four red giants in the globular cluster M13. The apparent wavelengths reflect the radial velocity of the cluster, i.e., ~247 km s^{-1}. The total exposure time of 120 minutes was composed of 3×40 minute exposures. The spectra are from Meszaros et al. (2009).

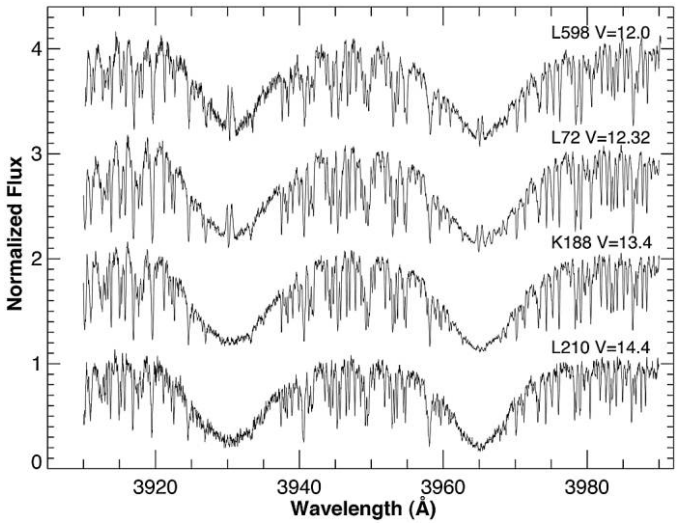

FIG. 21.—The Ca II H and K line region of four red giants in the globular cluster M15. The total exposure time of 120 minutes is divided into 40 minute segments. The spectra have not been binned. These spectra are from Meszaros et al. (2008).

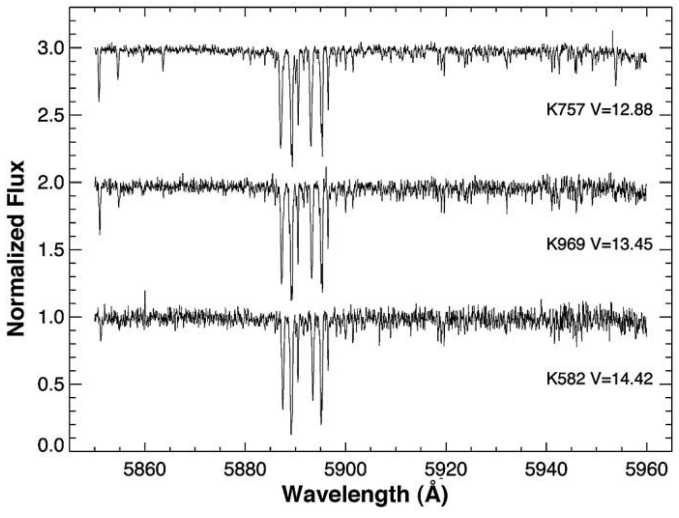

FIG. 22.—Detection of line-of-sight absorption by interstellar NaD is in the direction of M15. Both stellar and interstellar NaD absorption are evident in these spectra.

The Ca II doublet at 3933 Å and 3968 Å presents another set of challenges. The deep photospheric cores of the lines effectively cause the spectrum to be about 2 mag fainter than the visual magnitude of the star. We seek to detect and characterize the weak emission in the core of the line and to measure the position of H_3 and K_3—the central reversal of the emission cores. In this spectral region, the sky background can be important. Stellar spectroscopy generally is assigned to 'bright' time and the weak solar night sky spectrum also contains weak Ca II emission—similar to that found in red giants, which must be accounted for. Various techniques are used to determine the sky background. Many fibers can be placed on portions of the sky with no sources in order to obtain spectra with equivalent exposure time as the target objects. (Some observers choose to offset all of the fibers for an exposure on the sky following an exposure on targets.) With Hectochelle, we found a systematic variation of the sky exposures (after correcting the fibers for throughput) and so chose to form several averages of the sky spectra, depending on aperture. These were then subtracted from the spectra. Globular clusters generally have high radial velocities with respect to the local standard of rest, and so the Ca K cores of star and sky are well separated in wavelength.

The interstellar medium can be probed using the NaD filter with Hectochelle. Toward M15, there are several interstellar clouds at intermediate and high velocities (see Fig. 22) and the interstellar medium is quite patchy. With three exposures of 40 minutes each, and using various fiber configurations, material along the line of sight to the cluster core can be studied. With different fiber configurations on stars in the core of the cluster, reasonably high spatial mapping of the interstellar clouds can be accomplished.

12. DISCUSSION, CONCLUSIONS AND FUTURE PLANS

Hectochelle continues to be a workhorse instrument for the MMT observer community and is extremely popular with observers outside the MMT consortium that gain access to it through various guest-user programs. While fiber-fed spectrographs often suffer in comparison with slit-fed instruments, Hectochelle in fact has sensitivity close to that of slit-fed echelle spectrographs on telescopes with even larger apertures. This efficiency is due in large part to maximizing the throughput of the fiber feed system.

While we do not yet reach the PLDP level in radial velocity measurements, we get reasonably close and have demonstrated that we can achieve PLDP levels with advanced tunable laser calibrators. We plan to implement a permanent laser calibrator in the near future.

Cross-dispersion and an integral field unit for the Hectochelle have been discussed elsewhere (Szentgyorgyi et al. 2003; Fabricant et al. 2003b). Members of our group are completing a multislit optical spectrograph called Binospec (Fabricant et al. 2003a) that will supplant the role of Hectospec. At this time, the robot positioner will probably be retired. However, equipped with a cross-disperser and IFU, Hectochelle would be repurposed to a whole new science role, with selectable resolution and passband. With the extra space freed up if Hectospec were removed, it would possible to build a hyperinsulated thermally controlled enclosure for Hectochelle that would permit radial velocity precision near that of the HARPS spectrograph (Rupprecht et al. 2004), but mounted on a 6.5 m aperture telescope, nearly twice the size of the La Silla 3.6 m where HARPS is deployed.

TABLE 5
PROPERTIES OF ORDER-SORTING FILTERS AVAILABLE AT HECTOCHELLE

Filter	CWL (Å)	FWHM (Å)	Trans.	Trans CCD QE	Vendor	Included features
Ca 19	8580	450	0.96	0.38	Omega	Ca IR triplet
OB 21	7748	369	0.92	0.53	Omega	…
OB 24	6707	282	0.92	0.71	Omega	Li, [S II], He II
OB 25	6563	260	0.89	0.71	Omega	Hα, [N II]
OB 26	6632	241	0.89	0.71	Omega	…
Na 28	5892	208	0.87	0.73	Omega	Na D, He I
RV 31	5230	160	0.94	0.78	Barr	Radial velocity
OB 32	5007	159	0.87	0.73	Barr	[O III]
OB 33	4861	149	0.93	0.78	Barr	Hβ
OB 37	4351	119	0.98	0.79	Barr	[O III], Hγ
Ca 41	3950	96	0.96	0.72	Barr	Ca H&K

NOTE.—CWL is the center wavelength of the filter transmission band. FWHM is the full width at half-maximum of the passband. Trans. is the peak transmission of the filter, and Trans·CCD QE is the product of the peak transmission of the peak transmission and the focal-plane CCD quantum efficiency at transmission band center.

We are grateful for the contributions of the entire MMT instrument team and students and of the MMT and Whipple Observatory staff. We thank Kevin Bennett, David Bosworth, David Boyd, Daniel Blanco, William Brymer, David Caldwell, Shawn Callahan, Florine Collette, Emilio Falco, Craig Foltz, Art Gentile, Charles Hughes, Everett Johnston, Sheila Kannappan, Frank Licata, Steve Nichols, Dale Noll, Ricardo Ortiz, Tim Pickering, Frank Rivera, Phil Ritz, Cory Sassaman, Gary Schmidt, Dennis Smith, Ken Van Horn, David Weaver, Grant Williams and J. T. Williams. We thank the Robot positioner operators Perry Berlind and Mike Calkins and the MMT operators Mike Alegria, Alejandra Milone, and John McAfee. We are grateful to the efforts of the Harvard College Observatory Model Shop led by Larry Knowles. We thank Robert Dew and Diane Nutter of Cleveland Crystals and John Hoose of Richardson Grating Laboratory.

APPENDIX

ORDER-SORTING FILTER PROPERTIES

Twenty-five filters would be required to span the prime Hectochelle orders (orders 18 to 42, or ~3800 Å–9300 Å). Rather than procure a complete set of filters, we chose filters for orders containing the 11 most important spectral passbands. Among these was a special filter, RV31, designed to match the passband of other instruments used for Center for Astrophysics stellar radial velocity survey programs. The properties of the existing Hectochelle filters appear in Table 5.

REFERENCES

Avila, G., Guinouard, I., Jocou, L., Guillon, F., & Balszmo, F. 2003, Proc. SPIE, 4841, 997
Barnes, S. 2004, Ph.D. thesis, University of Canterbury (New Zealand)
Baxter, E. J., Covey, K. R., Muench, A. A., Furesz, G., Rebull, L., & Szentgyorgyi, A. H. 2009, AJ, 138, 963
Bershady, M., et al. 2008, Proc. SPIE, 7014, 7014H
Bohn, J. H., & Leist, R. W. 1998, Proc. SPIE, 3355, 962
Bottema, M. 1980, Proc. SPIE, 240, 171
Connes, P. 1985, Ap&SS, 110, 211
Conroy, M., Mandel, E., & Roll, J. B. 1998, in ASP Conf. Ser. 145, Astronomical Data Analysis Software and Systems VII, ed.. R. Albrecht, R. N. Hook, & H. A. Bushouse (San Francisco: ASP), 150
Cramer, C. E., Brown, S., Dupree, A. K., Korzennik, S. G., Lykke, K. R., & Szentgyorgyi, A. 2009, BAAS, 213, 611.05
Dekker, H., D'Odorico, S., & Fontana, A. 1994, ESO Messenger, 76, 16
Epps, H. W., & Vogt, S. S. 1993, Appl. Opt., 32, 6270
Fabricant, D. G., Epps, H. W., Brown, W. L., Fata, R. G., & Mueller, M. 2003a, Proc. SPIE, 4841, 1134
Fabricant, D. G., Hertz, E. H., & Szentgyorgyi, A. H. 1994, Proc. SPIE, 2198, 251
Fabricant, D. G., Szentgyorgyi, A. H., & Epps, H. W. 2003b, PASP, 115, 235
Fabricant, D. G., et al. 2004, Proc. SPIE, 5492, 767
Fabricant, D. G., et al. 2005, PASP, 117, 838
Fata, R. G., & Fabricant, D. G. 1998, Proc. SPIE, 3355, 275
Fata, R. G., Kradinov, V., & Fabricant, D. G. 2004, Proc. SPIE, 5492, 553
Furesz, G. 2008, Ph.D. thesis, University of Szeged (Hungary)
Furesz, G., Hartmann, L. W., Szentgyorgyi, A. H., Ridge, N. A., Rebull, L., Stauffer, J., Latham, D. W., Conroy, M. A., et al. 2006, ApJ, 648, 1090

Geary, J. 2000, in Further Developments in Scientific Optical Imaging, ed. M. B. Denton (Cambridge: Royal Soc. Chem.), 18
Hearnshaw, J. 2009, Astronomical Spectrographs and Their History (Cambridge: Cambridge Univ. Press), 83
Lu, G., Schoetz, G. F., Vydra, J., & Fabricant, D. G. 1998, Proc. SPIE, 3355, 884
Mateo, M., Olszewski, E. W., & Walker, M. G. 2008, ApJ, 675, 201
Meszaros, S., Dupree, A. K., & Szentgyorgyi, A. H. 2008, AJ, 135, 1117
Meszaros, S., Dupree, A. K., & Szalai, T. 2009, AJ, 137, 4282
Pickering, T., West, S., & Fabricant, D. G. 2004, Proc. SPIE, 5489, 1041
Roll, J. B., Fabricant, D. G., & McLeod, B. 1998, Proc. SPIE, 5489, 1041
Rupprecht, G., et al. 2004, Proc. SPIE, 5492, 148
Szentgyorgyi, A. H., Fabricant, D. G., Brown, W. R., & Epps, H. W. 2003, Proc. SPIE, 4841, 1026
Szentgyorgyi, A. H., et al. 2006, Hectochelle Observers Guide (Cambridge: CfA), http://www.cfa.harvard.edu/mmti/hectospec/Hectochelle_Observers_Manual.pdf
Szentgyorgyi, A. H., et al. 2008, Proc. SPIE, 7014, 70141W
Walker, M. G., Belokurov, V., Evans, N., Irwin, M. J., Mateo, M., Olszewski, E. W., & Gilmore, G. 2009, ApJ, 694, L144
Walker, M. G., Mateo, M., Olszewski, E. W., Bernstein, R., Sen, B., & Woodroofe, M. 2007, ApJS, 171, 398
Wolfe, J. D., &Thomas, N. L. 1999, Durable Silver Coating for Mirrors, US Patent 6,078,425 (filed 1999 June 9; issued 2000 June 20)